



Understanding the spatiotemporal dynamics of vegetation cover change (VCC) in the Teesta basin: a geospatial and statistical modelling-based investigation of environmental and human factors

Debarshi Ghosh¹ · Apurba Sarkar² · Sanjoy Mandal³

Received: 28 September 2023 / Accepted: 17 February 2025
© Saudi Society for Geosciences and Springer Nature Switzerland AG 2025

Abstract

This study presents an insightful analysis of vegetation cover change (VCC) within the Teesta Basin, utilizing various statistical models and geospatial techniques. The Ordinary Least Squares (OLS) regression model reveals a modest explanatory power with an adjusted R^2 of 0.1398, indicating its ability to account for approximately 13.98% of the variance in the data. This model, however, hints at potential heteroscedasticity and non-normal distribution of errors. In contrast, the geographically weighted regression (GWR) model, accounting for 84.556% of the variance, demonstrates a robust spatial heterogeneity in the relationships between the variables, offering a more nuanced understanding of the regional disparities. The study further incorporates a hot spot analysis using the Getis-Ord Gi* statistic, which exposes significant spatial clustering patterns in VCC, emphasizing the influence of both environmental and anthropogenic factors. The Boosted Regression Tree (BRT) model, with a substantial relative influence of 44.11% from 'Population Proximity', highlights the critical role of human-driven factors in vegetation dynamics. This model shows a moderate to strong correlation in predicting NDVI values. Analysis of seasonal trends reveals a cyclic pattern in NDVI values, indicating pronounced seasonal variations and negative trends in vegetation activity over time, particularly in the lower basin area. The Mann–Kendall time series analysis further confirms this declining vegetation trend. The study's findings are crucial for understanding the spatial and temporal dynamics of vegetation cover in the Teesta Basin. They underscore the importance of considering both environmental and human-driven factors in conservation strategies, especially in protected forest regions.

Keywords Vegetation cover change · Geographically weighted regression · Boosted Regression Tree · Spatial statistics · Non-parametric trend

Introduction

Responsible Editor: Biswajeet Pradhan

✉ Debarshi Ghosh
wetlanddeb@gmail.com

Apurba Sarkar
apurbasarkarugb@gmail.com

Sanjoy Mandal
sanjoymandal2392@gmail.com

¹ Department of Geography, Dhupguri Girls' College, Dhupguri, Jalpaiguri, West Bengal, India

² Department of Geography, Gour Banga University, Malda, West Bengal, India

³ Department of Geography & Applied Geography, University of North Bengal, Raja-Rammohunpur, Darjeeling, West Bengal, India

Extensive land-use change (LUC) has significantly impacted global ecosystems in recent decades, leading to alterations in biomass (Samadi et al. 2021), (Hussien et al. 2023) species diversity, vegetation cover (VC), and soil quality (Deng et al. 2013). These changes have a profound impact on the structure and functioning of ecosystems (Hussien et al. 2023). Landuse-cover practices vary worldwide but generally aim to exploit natural resources for human needs, often resulting in environmental degradation (Ranjan et al. 2022). Population growth and food production-related transformations exert pressure on protected areas, while conservation efforts aim to mitigate the negative effects of these changes (Zhao et al. 2022). The conservation of ecologically and culturally significant regions is crucial in preserving valuable ecosystem services (Tang et al. 2021). Vegetation cover plays a

crucial role in the interactions between land and atmosphere, impacting the energy, momentum, and hydrologic balance of the land surface. This close coupling between land and atmosphere influences the dynamics of the entire system (Pei et al. 2021). The relationship between ecosystems and climate operates on various timescales, from seconds to millions of years, encompassing both short-term responses of vegetation and soil to atmospheric processes and long-term evolution of ecosystems and soil structure (Haque and Basak 2017; Chughtai et al. 2021). However, anthropogenic activities introduce additional complexities by exerting external forces on such forest areas. Land use transformation, land management practices, and human activities have the potential to affect forest areas around the world at both local and global scales (Vrieling et al. 2011; Lawer et al. 2013; Feng et al. 2021).

Satellite images with high periodicity and low resolution, such as AVHRR (Holben 1986; Ohana-Levi et al. 2019a), SPOT and MODIS Normalized Difference Vegetation Index (NDVI) data are valuable for monitoring land-cover conditions and changes over large areas (Justice et al. 2002). According to the Pathfinder AVHRR Land Science Working Group, the development of global NDVI data sets was given the highest priority on a planetary scale (Defries et al. 1995). The NDVI has grown to be the most widely used index for rating vegetation because of its popular history, simplicity, and reliance on easily accessible multi-spectral bands (Shimu et al. 2019; Huang et al. 2021). MODIS NDVI processing, aimed at vegetation monitoring, utilizes cutting-edge remote sensing technology (Gu et al. 2007; Filippone et al. 2018; Baeza and Paruelo 2020; Zhang and Ye 2020). These multi-temporal datasets enable land-cover mapping, change detection and analysis of vegetation dynamics at regional and global scales (Gandhi et al. 2015). MODIS data provides standard vegetation indices like NDVI and Enhanced Vegetation Index (EVI) (Li et al. 2010) at different spatial and temporal resolutions, allowing for consistent comparisons of vegetation conditions and quantification of inter-annual variations (Yan et al. 2015). Instead of the spatial and spectral domains, the time domain is a better place to explore and analyse the temporal patterns of forest cover (Wellmann et al. 2020). Forest cover change in the corresponding local area may be indicated by changes in the temporal dynamics of satellite imagery pixels (Liu et al. 2018). To analyse temporal patterns, a number of methods have been suggested, including statistical ones like seasonal autoregressive integrated moving average (Zhang et al. 2011), PCA (Lasaponara 2006), monotonic and harmonic time series trend (Chamberlain et al. 2021) as well as signal processing ones like Fourier transform and wavelet analysis (de Jong et al. 2011). These techniques aid in comprehending and spotting changes in land cover over time (Detsch et al. 2016). Recuero et al. (2019) introduced

harmonic analysis to better understand and model periodic patterns in time series data. This decomposition involves four variables: level, frequency, amplitude, and phase, which describe the seasonal variations observed. Bokusheva et al. (2016) proposed the vegetation condition index (VCI) and the temperature condition index (TCI) to monitor drought conditions. NDVI, derived from satellite imagery, has been extensively utilized in previous studies to monitor vegetation health and assess the impacts of weather and climate changes (Pan et al. n.d.; Jiang et al. 2017; Bento et al. 2020).

Remote sensing is widely used to analyse and quantify the temporal and spatial trends of Land Use Change (LUC) and Vegetation Cover Change (VCC) (Yang et al. 2003; Abd El-Kawy et al. 2011; Wang et al. 2020). It is particularly efficient in conducting time-series analysis of Vegetation cover. VCC can be attributed to multiple factors related to residential development, including agricultural expansion, livestock production, and military activities (Singh et al. 2016; Baeza and Paruelo 2020). These activities can have diverse impacts on nearby protected nature reserves. Various methods have been utilized to estimate Vegetation Cover Change (VCC) using remotely sensed data, including multiple regression analysis, *k*-nearest neighbour, artificial neural network (ANN), and support vector machine (SVM) techniques (Huang et al. 2017; Silveira et al. 2019). The ANN model, known for its ability to handle complex nonlinear functions, has been successfully applied in land observation applications (Abdollahi et al. 2019). However, the accuracy of the ANN model can be compromised when there are insufficient samples or an excessive number of samples, leading to overfitting (Cui et al. 2020). In contrast, SVM, based on the principle of structural risk minimization is adept at solving practical problems involving limited training samples, non-linearity, high-dimensional data, and local minima (Zheng et al. 2015). Several studies have demonstrated the robustness of VCC and biomass estimation using SVM models (Filella et al. 2004). Quadrat surveys are limited in their applicability to large regions or scales, prompting the use of the Maximum Value Composite (MVC) technique for calculating annual maximum NDVI values (Taddei 1997). Previous reviews have explored vegetation cover change and its influencing factors, but there is a lack of recent research on large-scale anthropogenic factors that directly or indirectly affect vegetation cover change in North Bengal, India. Summarizing these factors and understanding their impact on positive or negative changes in vegetation cover would be valuable.

In the realm of environmental research, the study of vegetation cover change (VCC) has garnered significant attention due to its implications on climate change and sustainable landscape management (Hulley et al. 2014). A series of recent studies have contributed to this field by investigating the complex interactions between VCC, climatic variables,

and human activities. One study revealed notable correlations between vegetation indices, urban land proportions, rainfall, and temperature, underscoring the necessity for sustainable management of landscapes. Another significant research in Ethiopia assessed the impact of VCC on rainfall and land surface temperature, using advanced tools like NDVI, CHIRPS and MODIS data (Nega et al. 2019). This study highlighted a substantial loss of vegetation over 32 years, establishing a link with climatic alterations despite the absence of significant overall trends. Further contributing to this domain, the paper evaluated the effectiveness of VCC algorithms using MODIS 250-m data, examining land cover changes attributed to both human and natural factors in five distinct cases from the year 2000 (Zhan et al. 2002). The need for refinement in these methods was emphasized for future enhancement of VCC products. Additionally, a novel framework was introduced to analyse VCC in drylands, with a case study focusing on Israel's arid region (Ohana-Levi et al. 2019a). The research background in vegetation cover change highlights the significant role of NDVI in understanding seasonal and long-term trends. Studies have effectively used NDVI data to observe land degradation and regeneration in Mongolia, analysing factors like deforestation and climate variations (Eckert et al. 2015). Similarly, in Spain and the Balearic Islands, NDVI data revealed variations in vegetation trends by land-cover and climate types (Novillo et al. 2019). In China, NDVI indicated increases in vegetation, particularly in spring, influenced by climate and human activities (Piao et al. 2003). Lastly, in the Yucatán Peninsula, NDVI linked land use changes to seasonal greenness patterns, emphasizing human impact over climatic factors (Neeti et al. 2012). These studies collectively underscore NDVI's value in assessing vegetation changes across different regions. In India, studies focusing on basin-scale vegetation cover dynamics using long-term NDVI trends are rare, indicating a need for more comprehensive research in this area to understand the country's vegetation patterns.

Sikkim, which makes up a significant portion of the Teesta basin, lost 269 hectares of primary humid forest between 2002 and 2021. This loss accounted for 18% of Sikkim's overall loss of tree cover during that time (Tambe et al. 2011; Harris et al. 2021). The area of humid primary forest in Sikkim decreased by 0.53% in the same timeframe (Chakraborty et al. 2018). Overall, Sikkim lost 1.56 thousand hectares of tree cover from 2001 to 2021, representing a 0.62% decrease since 2000 (Mishra et al. 2020 and Hansen et al. 2012). Two regions in Sikkim were responsible for 65% of the tree cover loss between 2001 and 2021, with North Sikkim leading the way with 716 hectares lost, surpassing the average of 390 hectares (Kanade and John 2018). Moreover, Sikkim experienced a significant 100% decrease in relative tree cover, amounting to 1.56 thousand hectares lost since 2000, which accounted for less than 0.1%

of the global total (Sundriyal and Sharma 1996). Interestingly, the top two regions in Sikkim contributed to 71% of all tree cover gain between 2000 and 2020, with East Sikkim leading in tree cover gain at 27.6 hectares, surpassing the average of 17.4 hectares (Zhang et al. 2011; Hansen et al. 2013; Turubanova et al. 2018; Devi et al. 2021; Forest Declaration Assessment Partners 2022).

This study proposes a framework to examine the effects of environmental and human-driven factors on vegetation cover change (VCC) in the entire Teesta Basin in India (Traore et al. 2015; Ohana-Levi et al. 2019b). The novelty lies in its multi-decade trend analysis, spatial-temporal mapping and integration of modern methods to identify hotspots of VCC and their underlying causes. These findings aim to bridge the research gap in basin-scale vegetation studies in India, contributing to sustainable land-use practices and conservation strategies. The research focuses on understanding the changes in vegetation cover change (VCC) over time by analysing trends and determining their underlying causes. This study aims to evaluate the impacts of various factors on VCC, considering a span of multiple decades, and specifically includes protected nature reserves and forests within the basin. The specific objectives of the research are as follows: (1) generating a map that illustrates the spatial and temporal trends of VCC using 20 years of MODIS satellite imagery (2002 to 2022), (2) examining the primary environmental and human-driven factors that influence the trends in vegetation cover, and (3) identifying protected forest areas within the basin where significant changes in VCC are observed.

The study area

The Teesta River, stretching across a length of 414 km (257 mi), originates from the eastern Himalayan Pauhunri Mountain (Kundu et al. 2012). It meanders through the Indian states of Sikkim and West Bengal before crossing into Bangladesh through the Rangpur division. Eventually, it joins the Brahmaputra River in Bangladesh, which further merges with other significant rivers in the Bengal delta before flowing into the Bay of Bengal (Choudhury 2016). The Teesta river covers a substantial drainage area of 12,540 km² and traverses various regions including Mangan, Gangtok, Pakyong (Sikkim), Kalimpong, Darjeeling, Jalpaiguri, and Cooch Behar (West Bengal) in India (Chakraborty and Ghosh 2010) (Fig. 1). The Teesta river exhibits diverse landforms characterized by narrow valleys, rocky terrain, and steep slopes (Pal and Pani 2016). Its intricate network of streams, rivulets, and tributaries contribute to the overall drainage system, significantly shaping the landscape. The upper basin of the Teesta River receives water from streams originating in Tso Lhamo Lake, Gurudongmar Lake, as well

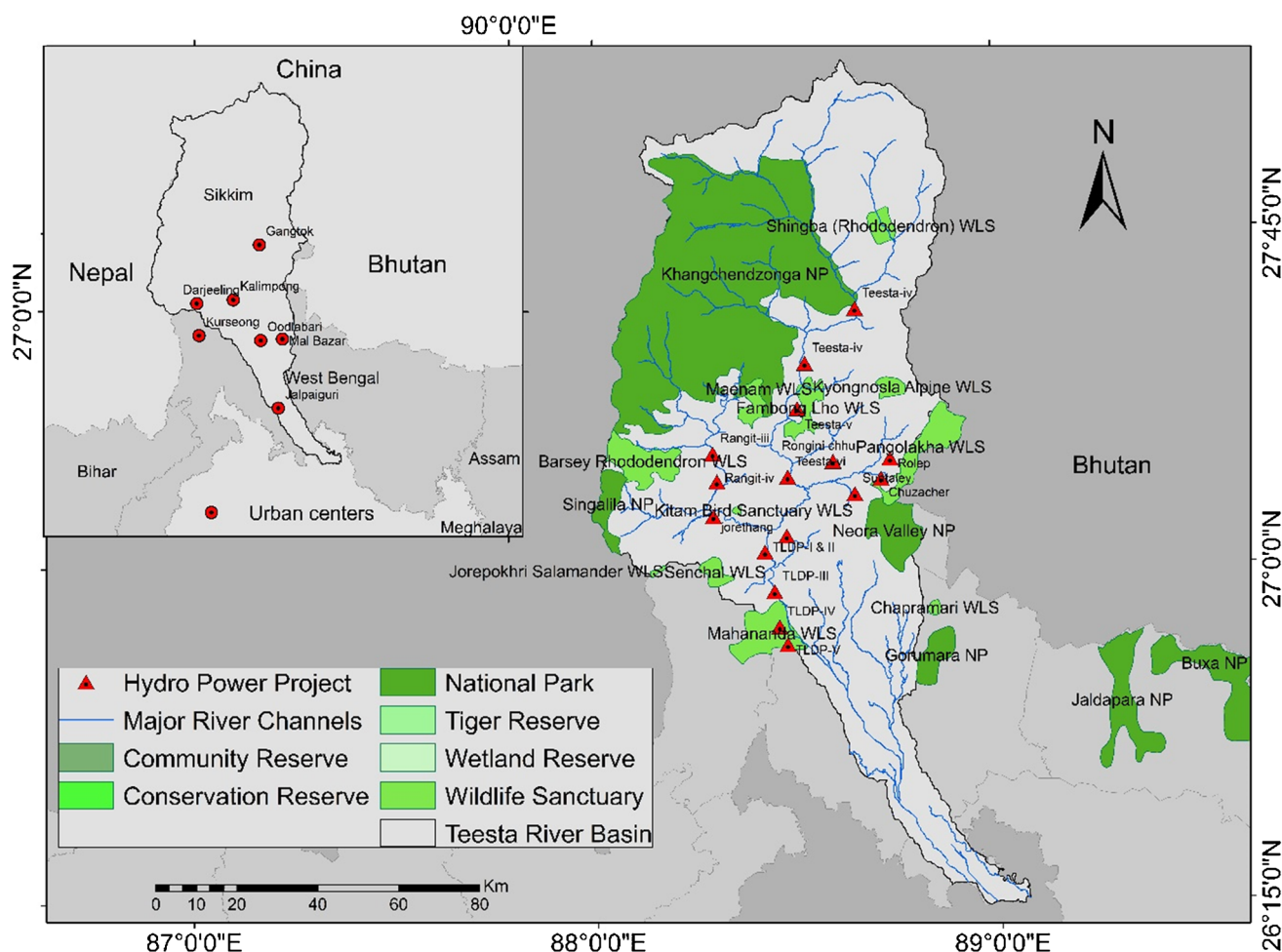


Fig. 1 Location of the study area

as rivulets stemming from the Thangu Valley, Yumthang Valley of Flowers, Dikchu, and Donkha mountain ranges (Krishna 1996). The described region encompasses various habitats, such as rocky and icy terrain, as well as Terai-Duar savannas and grasslands (Kulkarni et al. 2011). It consists of diverse biomes, including Tundra, as well as Tropical and Subtropical Grasslands, Savannas, and Shrublands (Singh et al. 2010). The majority of the region is comprised of land, with an area of 2.31 million hectares situated in a combination of lowland and mountainous areas. Between the years 2002 and 2020, the Teesta basin in India experienced a gain of 41.3 thousand hectares in tree cover, accounting for approximately 1.8% of its total extent.

As it flows through Melli and towards Teesta Bazaar, the Teesta River serves as the border between Sikkim and West Bengal below Rongpo. (Karim and Thiel 2017). Just before the Teesta Bridge, where roads from Kalimpong and Darjeeling converge, the river encounters its largest tributary, the Rangeet River (Sarkar et al. 2021). Continuing its course, the Teesta River enters the plains at Sevoke (near

Siliguri), where it is spanned by the Coronation Bridge and Sevoke Railway Bridge (Talukdar et al. 2021). These bridges are crucial for connecting India's north-eastern states to the rest of the nation (Mondal et al. 2020). The river travels through the Jalpaiguri district further downstream before passing through the Cooch Behar district's Mekhliganj and Haldibari.

The Teesta basin is home to numerous national parks and wildlife sanctuaries, including Khangchendzonga National Park (Sikkim), Singalila National Park, Neora Valley National Park, Jaldapara National Park, and Mahananda Wildlife Sanctuary (West Bengal), among others (Table 1). In the Teesta Basin, significant changes in vegetation cover (VC) have been observed, particularly in the upper basin (Ghosh 2021). These changes include an increase in agriculture and pasture lands, as well as a decline in primary forests (Broad and needle-leaved coniferous and deciduous forests). Recent field visits to Sikkim help us to understand how the recent construction of roads and rail lines throughout the basin has resulted in the segregation and loss of primary

Table 1 State-wise distribution of National parks (NP) and Wildlife sanctuaries (WLS)

State	NP/WLS	Area (in Sq. km.)	State	NP/WLS	Area (in Sq. km.)
Sikkim	Khangchendzonga NP	1748.00	West Bengal	Neora Valley NP	159.89
Sikkim	Fambing Lho WLS	51.76	West Bengal	Gorumara NP	79.45
Sikkim	Kyongnosla Alpine WLS	31.00	West Bengal	Singalila NP	78.60
Sikkim	Maenam WLS	35.34	West Bengal	Jorepokhri Salamander WLS	0.04
Sikkim	Shingba (Rhododendron)	43.00	West Bengal	Senchal WLS	38.88
Sikkim	Kitam Bird Sanctuary WLS	6.00	West Bengal	Mahananda WLS	158.04
Sikkim	Barsey Rhododendron WLS	104.00	West Bengal		
Sikkim	Pangolakha WLS	128.00	West Bengal		

Source: Calculated from the ESRI Arc GIS online data

and secondary forests (Woodland savannah). These findings provide important insights into the dynamics of VC changes and their impact on the ecosystem within the Teesta Basin. The Sikkim region comprises various habitats such as Eastern Himalayan broadleaf forests and Himalayan subtropical pine forests (Sultana et al. 2018). Notably, there are no intact forests in this area. The prevailing climate in most parts of the region is warm and temperate, characterized by dry winters and warm summers. Additionally, there are areas with a warm and temperate climate featuring dry winters and hot summers. The region encompasses different biomes, including Temperate Broadleaf and Mixed Forests, as well as tropical and subtropical coniferous forests.

Methods and materials

Time series analysis of normalized NDVI

This methodology (Fig. 2) focuses on identifying significant trends in the Teesta Basin's Normalized Difference Vegetation Index (NDVI) time series. 20 MODIS (Zhan et al. 2002; Miller and McKee 2004) satellite images from the MOD13Q1 V6.1 product (Table 2), spanning a 20-year time period from 2002 to 2022, were pre-processed in the Google Earth Engine platform (Hansen and Loveland 2012). For each image, the Normalized Difference Vegetation Index (NDVI) was computed (Simoniello et al. 2008). The individual NDVI images were then combined into a single band to create the 20-year mean NDVI, allowing for time series analysis (Klein et al. 2012). The NDVI formula commonly used for MODIS Terra Collection 250-m images is as follows:

$$\text{NDVI} = \frac{\text{NIR}(\text{band 5}) - R(\text{band 4})}{\text{NIR}(\text{band 5}) + R(\text{band 4})}$$

Here, NIR represents the reflectance value of near-infrared light (1.230 to 1.250 μm) and Red represents the reflectance value of red light (0.640 to 0.670 μm). The reflectance

values are typically obtained from the MODIS Terra Collection 250-m images, which provide measurements of these spectral bands (Chen et al. 2007, 2015).

The vegetation cover change modelling involved the use of statistical regression-based models. Various factors were considered, including environmental factors (Fig. 3a, b, c, d, e, and f) like slope, slope aspect, land cover classes, land surface temperature, precipitation, soil erodibility, soil loss, mean soil moisture, and soil texture (Fig. 4a, b, c, and d). Additionally, human-driven factors (Fig. 5a, b, c, d, e, and f) such as distance to urban centres (DtUrban), distance to urban centres from night-time images (Nig_Urb), distance to population (DtP), distance to the dam (DtDm), and distance to the road (DtRd) were also taken into account. These factors served as explanatory variables to analyse their impact on vegetation cover change (VCC), represented by the Normalized Difference Vegetation Index (NDVI).

The model examined the use of the Contextual Mann–Kendall (CMK) significance test to find spatiotemporal trends in VCC (Yue and Pilon 2004; Neeti and Eastman 2011). The Contextual Mann–Kendall (CMK) significance test, which takes into account spatial information and makes use of the Theil-Sen (TS) slope estimator, is used in the analysis (De Beurs and Henebry 2005; Zhang et al. 2008). While taking neighbouring pixel values and spatial autocorrelation into account, the goal is to identify and quantify estimated NDVI trends (Fig. 6a). To ensure consistency and quality of the data, the Teesta Basin's NDVI time series data is first collected for a specific time period and put through pre-processing procedures. These actions entail cleaning the data, locating outliers, and possibly aggregating the data over time. The steps of the CMK test are as follows: (1) Ranking and Pairwise Comparisons: The NDVI time series data are ranked according to the passage of time, creating a temporal hierarchy of observations (Ahmad et al. 2015). (2) Theil-Sen Slope Estimator: Theil-Sen slope estimators are computed for every pixel by taking into account all potential pairwise combinations of observation values (Peng et al. 2008). The trend between adjacent pairs of time steps is represented

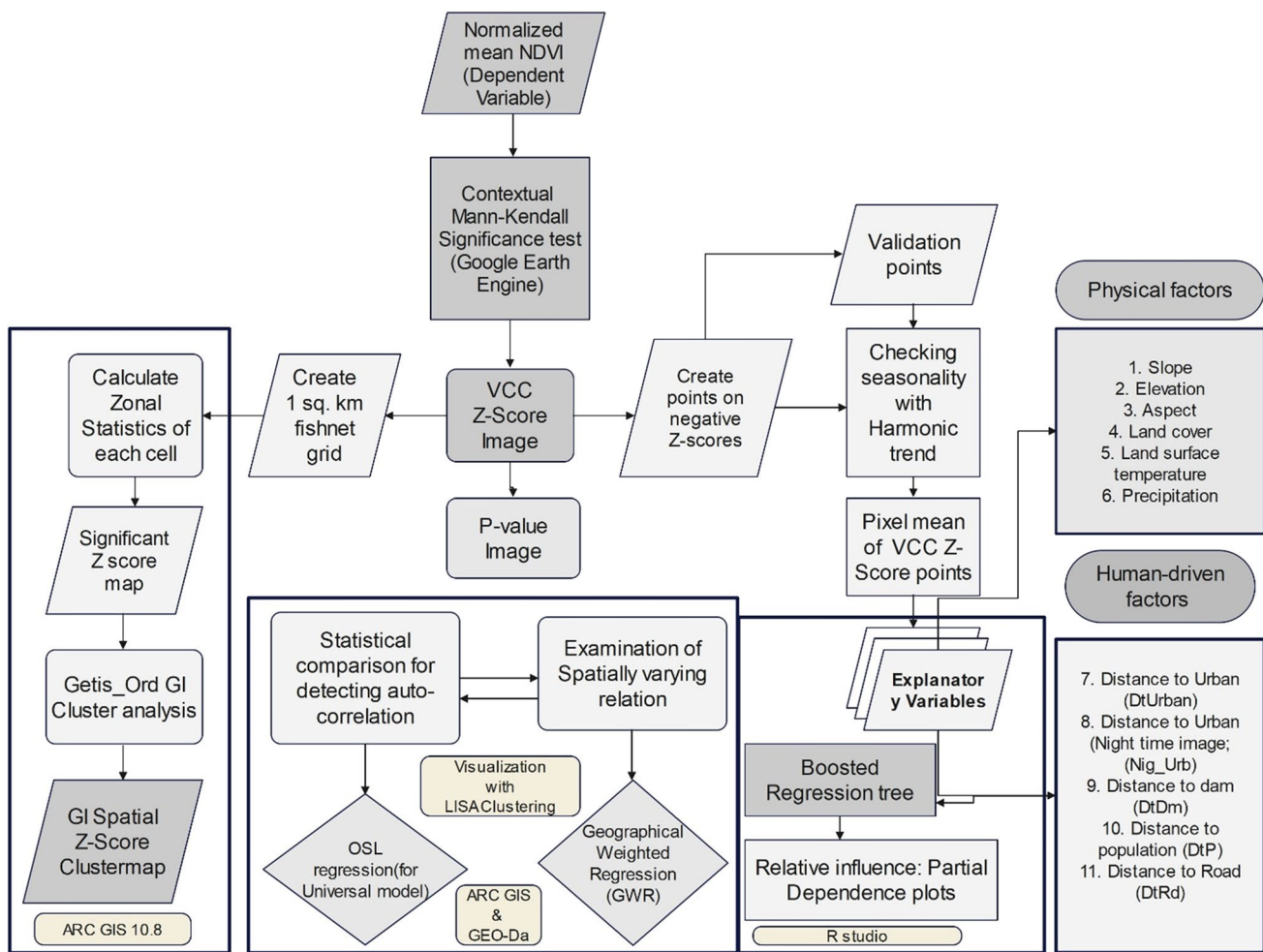


Fig. 2 Methodological flow diagram of the work

by a set of slopes in this. (3) Contextual Neighbourhood: A 3×3 neighbourhood is considered for each pixel in order to minimise biases and take into account spatial autocorrelation (Qin et al. 2021). The pixel being analysed serves as the reference, and the NDVI values of its surrounding pixels are contrasted with those of the reference pixel at corresponding time steps. (4) CMK statistic: The ranked NDVI values and Theil-Sen slopes (Fig. 6b) are used to calculate the CMK statistic. (5) VCC z-score: The Vegetation Cover Change (VCC) z-score (Fig. 6c) is calculated to further standardise the CMK statistic. This z-score has a normal distribution with a mean of 0 and a standard deviation of 1, making it possible to determine the trend's direction and statistical significance. (6) Calculation of p-value: The normal cumulative distribution function is used to calculate the p-value for the CMK statistic. P-values 0.05 indicate a significant trend (Fig. 6d), with a significance level of 0.05 (confidence limit of 95%). (7) VCC z-score map: The resulting VCC z-score map shows how the magnitude and direction of the NDVI trend are distributed spatially within the Teesta Basin.

While negative scores show declining trends, positive scores show increasing trends. In conclusion, this study effectively detects and quantifies significant trends in vegetation dynamics by applying the CMK significance test to the NDVI time series in the Teesta Basin. To determine the size and direction of the trends, the methodology uses the Theil-Sen slope estimator, spatial autocorrelation, and contextual geographic data. The resulting VCC z-score map offers insightful information about the geographic distribution of NDVI changes (Li et al. 2013; Gillespie et al. 2018; Lin et al. 2020).

Comparison and visualization

To better comprehend the temporal changes in the predicted response variable, a regression-based comparison was carried out using Ordinary Least Squares (OLS) regression (Fig. 7a, b, c, d, e, f, and g) and Geographically Weighted Regression (GWR) (VCC) (Erdoğan 2010; Devkota et al. 2014). The regression modelling process employed a systematic approach, beginning with Ordinary Least Squares

Table 2 Database used in the study

Parameters	Data type	Description	Source
Digital surface model	Raster Geo-TIFF (fully compliant with TIFF version 6.0)	GLO-30 offers global coverage at a resolution of 30 m	https://spacedata.copernicus.eu/collections/copernicus-digital-elevation-model
Precipitation (mm/day) (11 years mean)	Raster CHIRPS Daily: Climate Hazards Group Infrared Precipitation With Station Data (Version 2.0 Final)	5566 m resolution	https://chc.ucsb.edu/data/chirps
Land-surface temperature (unit in Kelvin)	Raster (mean of 20 years)	The MOD11A2 V6.1 product provides an average 8-day land surface temperature (LST). Scale factor 0.02, resolution 1000 m	https://lpdaac.usgs.gov/products/mod11a2v061/
MODIS land cover type yearly	Raster (2022)	The Terra and Aqua Combined Moderate-Resolution Imaging Spectroradiometer (MODIS) Land Cover Type (MCD12Q1) version 6.1 data product, LC type 2; resolution, 500 m	https://lpdaac.usgs.gov/products/mcd12q1v061/
World global project population data	Raster (2022)	Resolution, 92.77 m	https://www.worldpop.org/
Terra vegetation indices 16-day global (NDVI)	Raster (mean of 20 years)	Resolution, 1000 m; scale factor, 0.0001	https://lpdaac.usgs.gov/products/mod13a2v061/
Road layers	Vector (line data)	Open street map data	https://www.openstreetmap.org/#map
Dams	Vector (point data)	GLOBAL georeferenced Database of Dams GOOD2 version 1	http://atlas.gwsp.org/
Wildlife protected areas in India (web layer)	Vector layer (polygon data)	National parks and Wildlife sanctuaries	ESRI India, ENVIS Centre on Wildlife & Protected Areas
Urban centres; night-time light intensity (nanoWatts/cm ² /sr)	Vector layer (point data); night-time satellite image (raster)	Traced from Google Earth Pro. Monthly average radiance composite images using night-time data from the Visible Infrared Imaging Radiometer Suite (VIIRS) day/night band (DNB)	https://earth.google.com; https://eogdata.mines.edu/download_dnb_composites.html
NDVI harmonic trend (2005–2022)	Raster layers (mean NDVI)	MODIS/006/MOD13A2; resolution, 500 m	https://lpdaac.usgs.gov/products/mod13a2v061/
SMAP level-4 (L4) soil moisture product	Raster layers	3-hourly time-averaged geophysical data	https://nsidc.org/data/spl4smgp/versions/7
Soil texture class (USDA system)	Raster layers	Resolution of 250 m at 0 cm depth	https://zenodo.org/records/2525817
Source: computed by the authors			

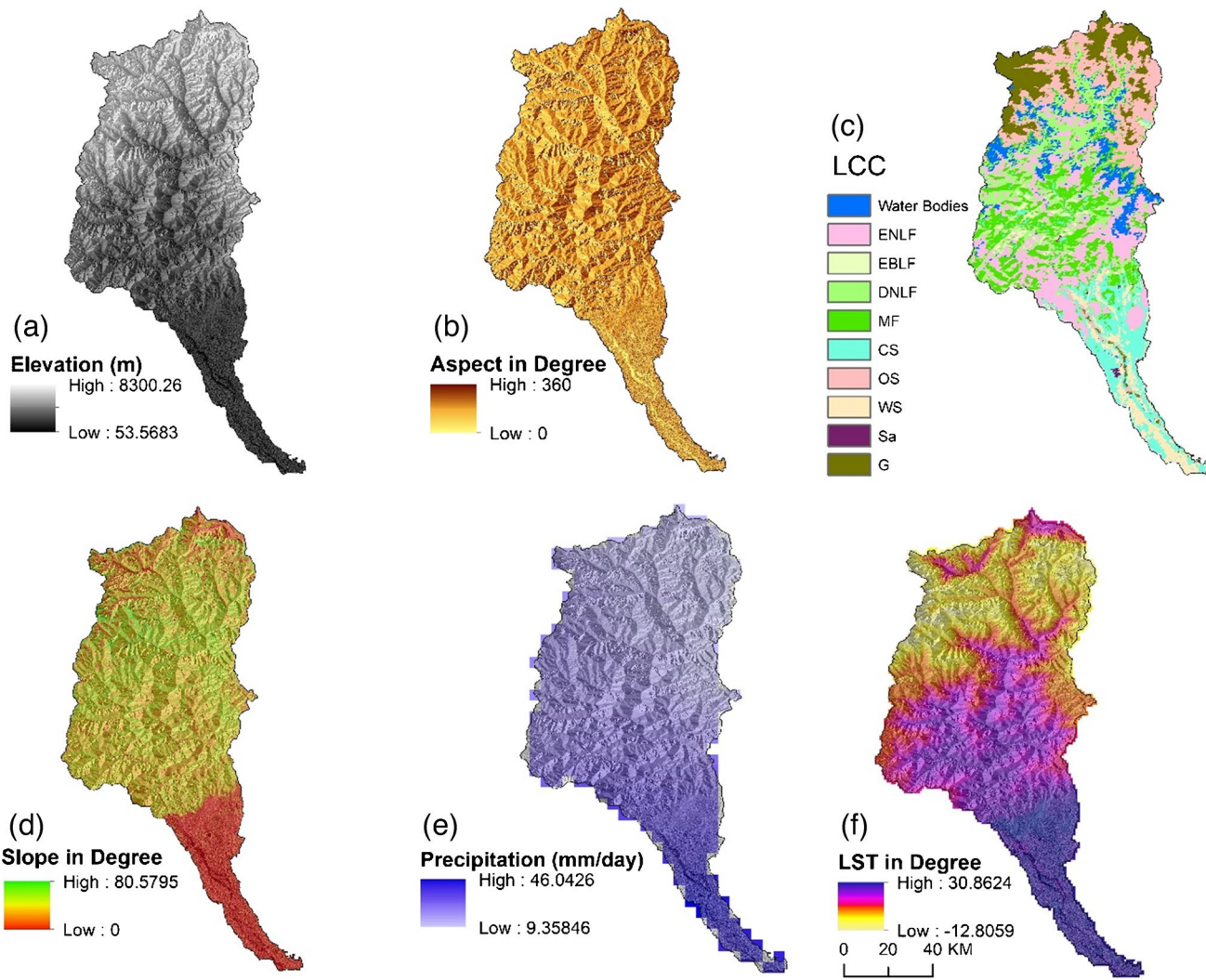


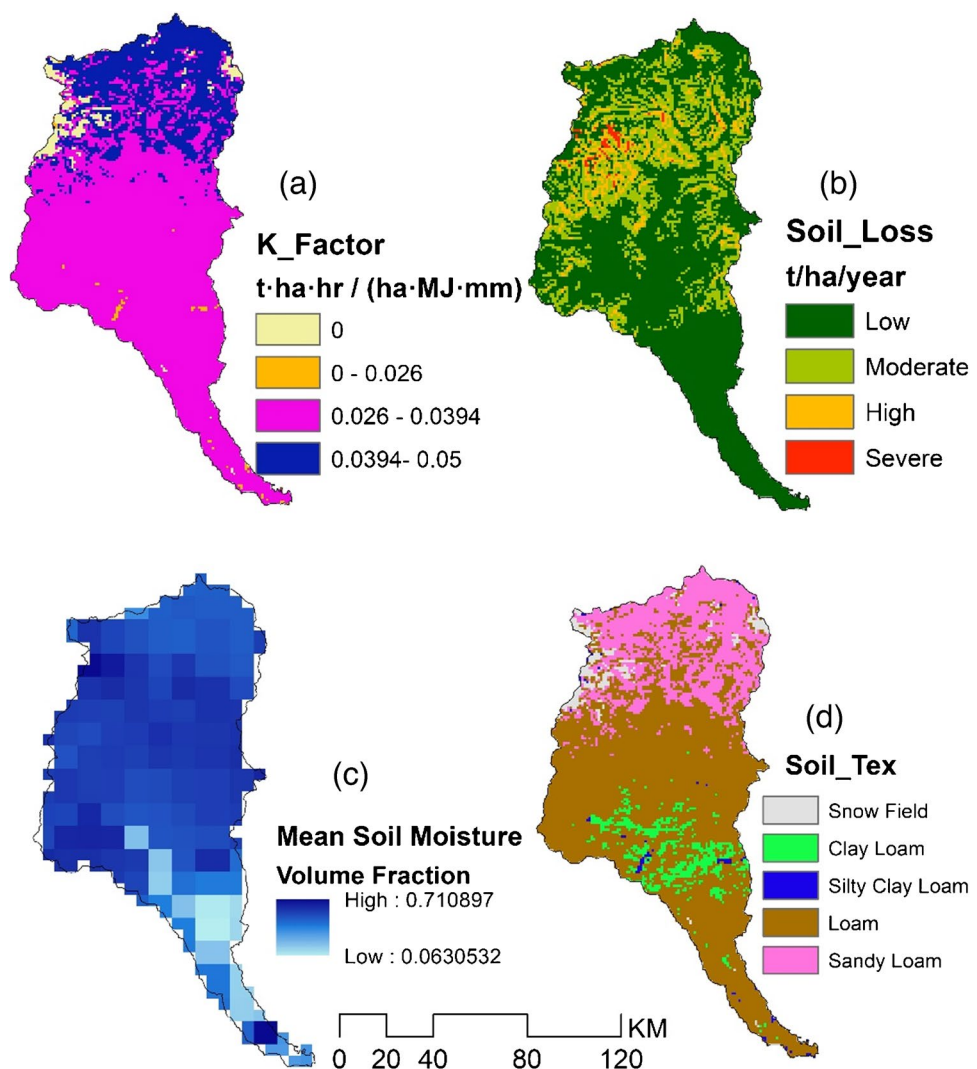
Fig. 3 Regression explanatory variables: **a** elevation (m), **b** aspect (degrees), **c** land cover classes (LCC), **d** slope (degree), **e** precipitation (mm day^{-1}), and **f** land surface temperature (K). LCC classes: ENLF, evergreen needle leaf forest; EBLF, evergreen broad leaf

forest; DNLF, deciduous needle leaf forest; MF, mixed forest; CS, closed savannah; OS, open savannah; WS, woodland savannah; Sa, savannah; G, grassland

(OLS) regression to analyse the relationships between NDVI and a range of physical (e.g., slope, precipitation, land cover) and human-driven factors (e.g., proximity to urban centres, population, dams, and roads). To refine the model, stepwise selection was used to iteratively optimize the Akaike Information Criterion (AIC), while Lasso regression applied regularization to prioritize the most significant predictors. Interaction terms were incorporated to capture context-specific dependencies, such as those between land cover and precipitation. Diagnostics, including Variance Inflation Factor (VIF) for multicollinearity and residual analyses for model assumptions, ensured robustness. The Variance Inflation Factor (VIF) analysis revealed high multicollinearity among certain predictors, particularly for Elevation (VIF = 12.09), DtP (VIF = 11.91) and LST (VIF = 14.29),

indicating potential redundancy in the explanatory variables. To address this, Lasso regression was employed to penalize less important predictors, effectively reducing multicollinearity and ensuring that the overall model retained only the most influential variables, thus maintaining robustness and interpretability. In both the simple Ordinary Least Squares (OLS) and Geographically Weighted Regression (GWR) models, we have incorporated various physical-driven factors, including slope, precipitation, land cover classes and land surface temperature (Table 2). Additionally, we have included a set of human-driven explanatory variables such as distance to urban centres (derived from Landsat imagery and night-time sensitivity image), population, dams, and roads. The predicted variable in our models is the Normalized Difference Vegetation Index (NDVI), representing the

Fig. 4 Regression explanatory variables: **a** soil erodibility factor (K), **b** soil loss, **c** mean soil moisture (MSM), **d** soil texture



mean value over a 20-year period (Table 2). The examination of how the relationship between predictor variables and VCC changed over various time scales was made possible by these regression models. Using Univariate Moran's *I* statistics (distance weight, uniform Kernel function) carried out in the Geo-Da statistical package, both the OSL and GWR models successfully predicted the NDVI values while capturing significant clustering patterns. The spatial patterns of the recognised vegetation trends were assessed using a cluster analysis of spatial statistics. In order to understand how vegetation changes are distributed spatially, this analysis sought to locate clusters or groups of pixels with comparable VCC patterns.

Estimate seasonality with harmonic trend

A harmonic model is used to represent the periodic patterns in a time series using sine and cosine functions. It consists of multiple sinusoidal functions with different frequencies

and phases, and the number of components depends on the observed periodicity of the data. The Fourier transform is used to estimate the coefficients of the harmonic model and fit it to the detrended NDVI time series (Ohana-Levi et al. 2019b; Ramanathan et al. 2020). The estimated seasonality component is obtained by evaluating the fitted harmonic model using the parameter estimates. The harmonic model of seasonality in NDVI uses sine and cosine functions to represent seasonal fluctuations in the NDVI values over time (Jakubauskas et al. 2001). The data is processed by adding an NDVI band and a time band representing fractional years, and the number of harmonic terms is determined by the variable 'harmonics' (Zhou et al. 2015; Padhee and Dutta 2019). The fitted model of seasonality in NDVI allows us to understand and quantify the periodic patterns and variations in vegetation activity captured by the NDVI time series data (Liu et al. 2017) in Google Earth Engine. This approach focuses on pixels where significant changes in z-values are identified through non-parametric trend analysis (Li et al.

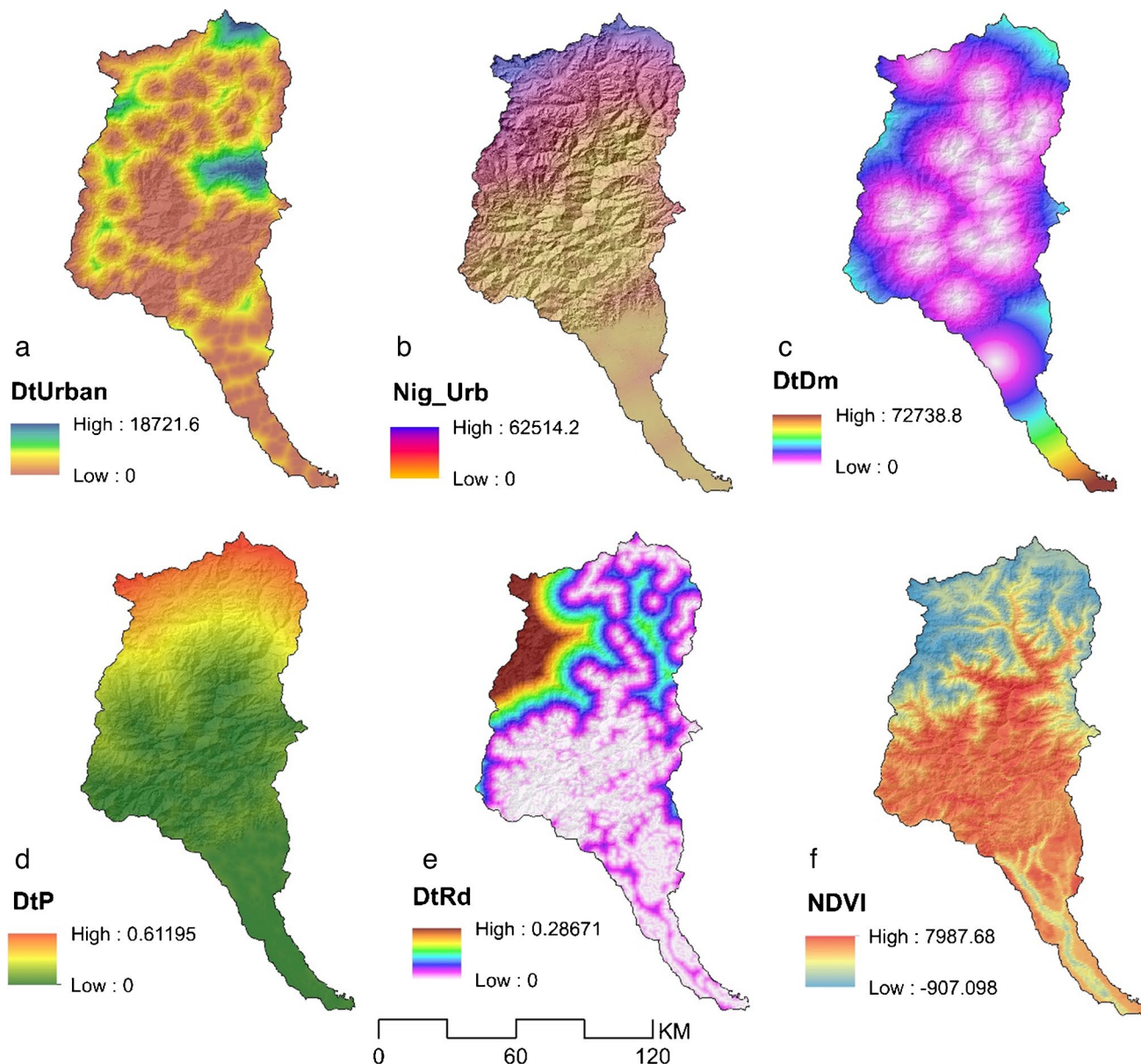


Fig. 5 Regression explanatory variables (human driven factors): **a** distance to urban (**DtUrban**), **b** distance to urban centres based on night time sensitivity of light (**Nig_Urb**), **c** distance to dam (**DtDm**), **d** distance to population (**DtP**), **e** distance to road (**DtR**), and **f** mean NDVI (20 years)

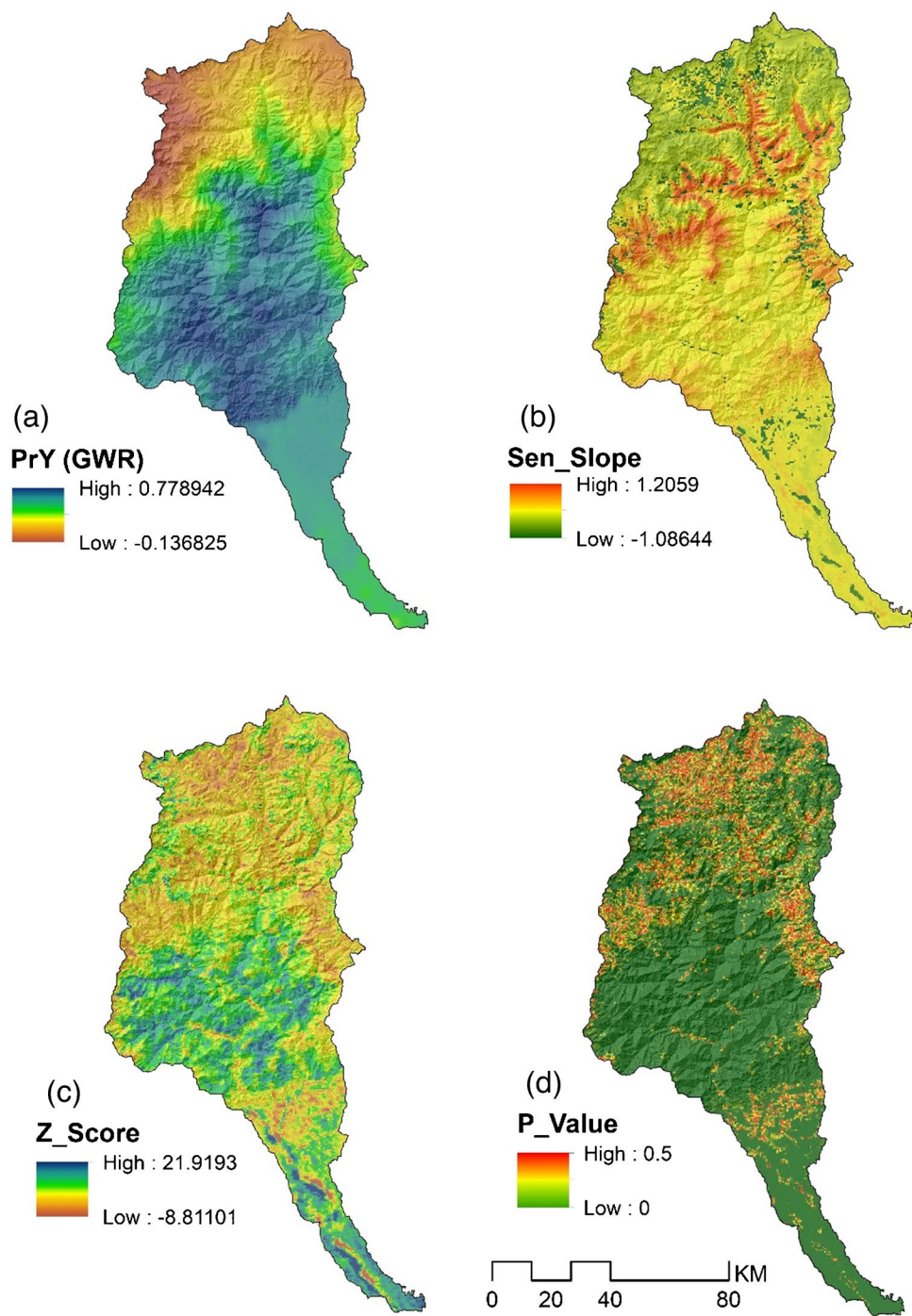
2021). The harmonic model of seasonality in NDVI is utilized as a tool to validate and cross-check the seasonal trends of NDVI fluctuations at specific pixels in the study area. This approach focuses on pixels where significant changes in z -values are identified through non-parametric trend analysis. The results showed positive Sen's slope dependency on explanatory variables in broad needle leaf forests (BNLF) in high mountain tracts (Khangchendzonga National Park) (Fig. 8a), moderate seasonal VCC with positive slope in evergreen broadleaf forest (EBLF) transition zones to Yuksum (within Khangchendzonga National Park and Barsey Rhododendron Wildlife Sanctuary) (Fig. 8b), transitional

VCC between mixed and deciduous needle leaf forests from Gangtok to far east (Fig. 8c), and finally, high seasonal VCC and negative slope trends can be observed within a transition zone from Woody Savannah (WS) to Grassland (G) over the piedmont section (Fig. 8d).

Interaction among human-derived factors

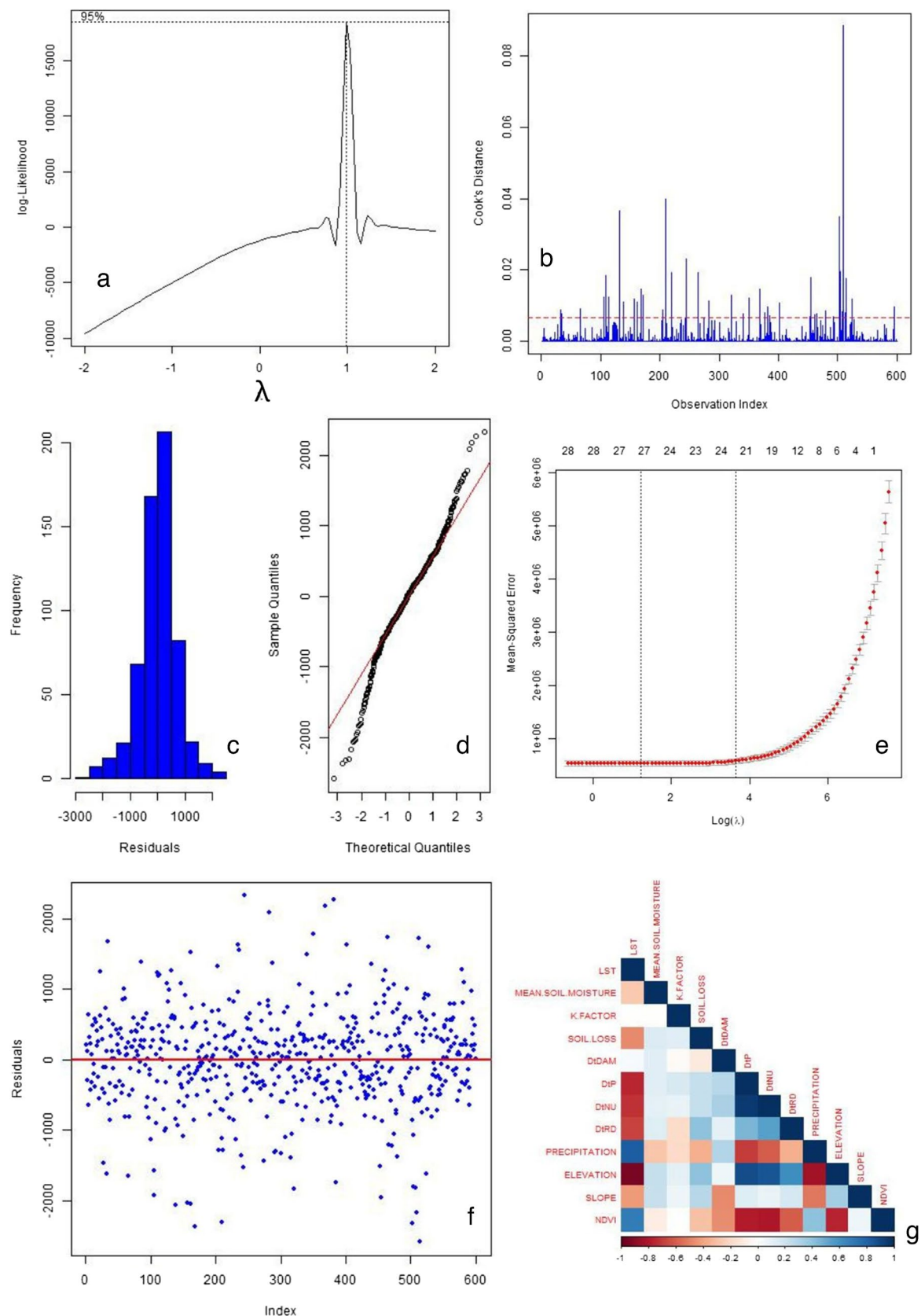
In this study, a Gradient-Boosted Regression Trees (BRT) algorithm (Klein et al. 2012; Manna et al. 2018; Ohana-Levi et al. 2019b) was employed to analyse the change in Normalized Difference Vegetation Index (NDVI) and assess

Fig. 6 Various model and trend analysis outcome: **a** Predicted y raster of GWR model, **b** Sen's slope raster, **c** z -score raster of CMK analysis, and **d** p -value raster of CMK analysis



the relative influence of various predictor variables on Vegetation Cover Change (VCC). The BRT algorithm, implemented using the ‘dismo’ package in R Studio, is a powerful machine learning technique capable of capturing complex interactions and non-linear relationships between predictors and the response variable (Gelman, 2012). The study considered five predictor variables to quantify the impact of human-driven factors on VCC. The response variable was the scaled NDVI, while the predictor variables included

distance to urban, road, dam, and population (Ojima et al. 1994). Through a relative importance graph, the BRT model provides useful insights into the most important human-derived factor affecting VCC. The BRT model configuration involved several parameters, such as the number of trees (1000), the family distribution (Gaussian), tree complexity (5), learning rate (0.04), and bag fraction (0.5) (Döpke et al. 2017; Ilic et al. 2021). These settings were optimized to ensure accurate and robust predictions of the scaled NDVI.



◀Fig. 7 OLS regression outcomes: **a** Box-Cox transformation plot indicating optimal λ , **b** Cook's distance plot identifying influential observations, **c** residual histogram assessing normality, **d** QQ plot of residuals for normality check, **e** Lasso cross-validation plot showing optimal λ , **f** residuals vs. index plot examining randomness, and **g** correlation matrix visualizing multi-collinearity

Moreover, the BRT model provides additional interpretability through Partial Dependency (PD) plots and Interaction plots (Riihimäki et al. 2017; Han et al. 2019). The model provides insights into the drivers of vegetation cover change through relative importance graphs, PD plots, and interaction plots.

Results

OLS regression

The Ordinary Least Squares (OLS) regression analysis was conducted to understand the relationship between NDVI (Normalized Difference Vegetation Index) and multiple predictors, including both categorical and continuous variables. The analysis revealed significant multicollinearity through Variance Inflation Factor (VIF) values, where LST (16.29), DtP (20.91), and Elevation (29.09) exhibited high correlations with other predictors, indicating potential distortions in coefficient estimates and a need for adjustments using techniques like Ridge or Lasso regression. Stepwise regression, employing forward and backward selection, optimized the model by retaining influential variables such as LULC, soil loss, DtDAM, precipitation, elevation, and slope while excluding negligible contributors like DtRD and K factor. The final stepwise model achieved an adjusted R^2 of 0.9117, explaining 91.17% of NDVI variance and offering a more streamlined representation of relationships while addressing redundancy. Incorporating interaction terms further highlighted significant dependencies, particularly between LULC and Precipitation ($\rho=0.00174$), emphasizing that the relationship between precipitation and NDVI is contingent on the land cover type. Although interactions such as LULC and Mean Soil Moisture (MSM) were less impactful, they provided additional insights into complex dependencies. The full OLS model, including all predictors, was consistent with the stepwise approach, achieving an adjusted R^2 of 0.9115 and identifying significant contributors, notably LULC categories (e.g., Evergreen Broadleaf Forests, Deciduous Needle leaf Forests, Mixed Forests, Open Shrublands, Savannas, and Grasslands), Soil Loss, DtDAM, Precipitation, Elevation and Slope (in every case p -value is less than 0.05). While the full model retained all predictors, the stepwise model proved more efficient by excluding irrelevant variables without compromising predictive power. Overall, land cover

types emerged as the most critical categorical predictors, and environmental factors like elevation, slope, soil loss, and precipitation significantly influenced NDVI. High multicollinearity among certain variables necessitates careful handling to improve robustness, and interaction effects between land cover and precipitation revealed deeper complexities in their relationships. The results underscore the importance of adopting the stepwise regression model for its balance of simplicity and predictive accuracy, offering a comprehensive understanding of the factors influencing NDVI variations (Fig. 7a, b, c, d, e, f, and g).

Geographically weighted regression (GWR) model

The GWR model, with an adjusted R^2 of 0.941, outperforms other models by effectively capturing local spatial variations, although it incurs higher residual squares (200,825,219.778) and AICc (7633.153) due to the complexity of spatial modelling. In contrast, the Full OLS model demonstrates robust global performance with a balanced adjusted R^2 of 0.916, low residual squares (3.811), and a residual standard deviation of 0.080, highlighting its efficiency in explaining global variability. The Stepwise model and Interaction model, with adjusted R^2 values of 0.9117 and 0.874, respectively, provide simplified frameworks that reduce multicollinearity but are less effective in accounting for the spatial and global variability captured by the GWR and OLS models. (Table 3).

Hot spot analysis

The spatial Getis-Ord Gi* statistic was used to evaluate the spatial interactions between the driver variables. The cluster analysis and hot spot analysis revealed distinct spatial patterns in the distribution of VCC scores across the study area (Fig. 9a). These patterns were then explored further through geographically weighted regression, identifying significant drivers of clustering (Fig. 9b), including both environmental and anthropogenic activity bases rasters. The IDW stretch of the standard error of the GWR model provides additional insights into these patterns (Fig. 9c). Finally, the temporal trend of clustering (Getis-Ord Gi*) in vegetation cover was analysed to understand the dynamics over time (Fig. 9d). To investigate the connections between the Getis-Ord Gi* results and nine environmental and human-driven factors, a spatial correlation analysis was carried out. The GiZ score measures how far the observed spatial pattern of a variable deviates from what would be expected under spatial randomness. A positive GiZ score suggests the presence of clustering, meaning that areas with similar attribute values tend to be located close to each other. It indicates whether the variable exhibits clustering (positive GiZ score), dispersion (negative GiZ score), or randomness (GiZ score close to zero). The result was an adjusted regression (R) value,

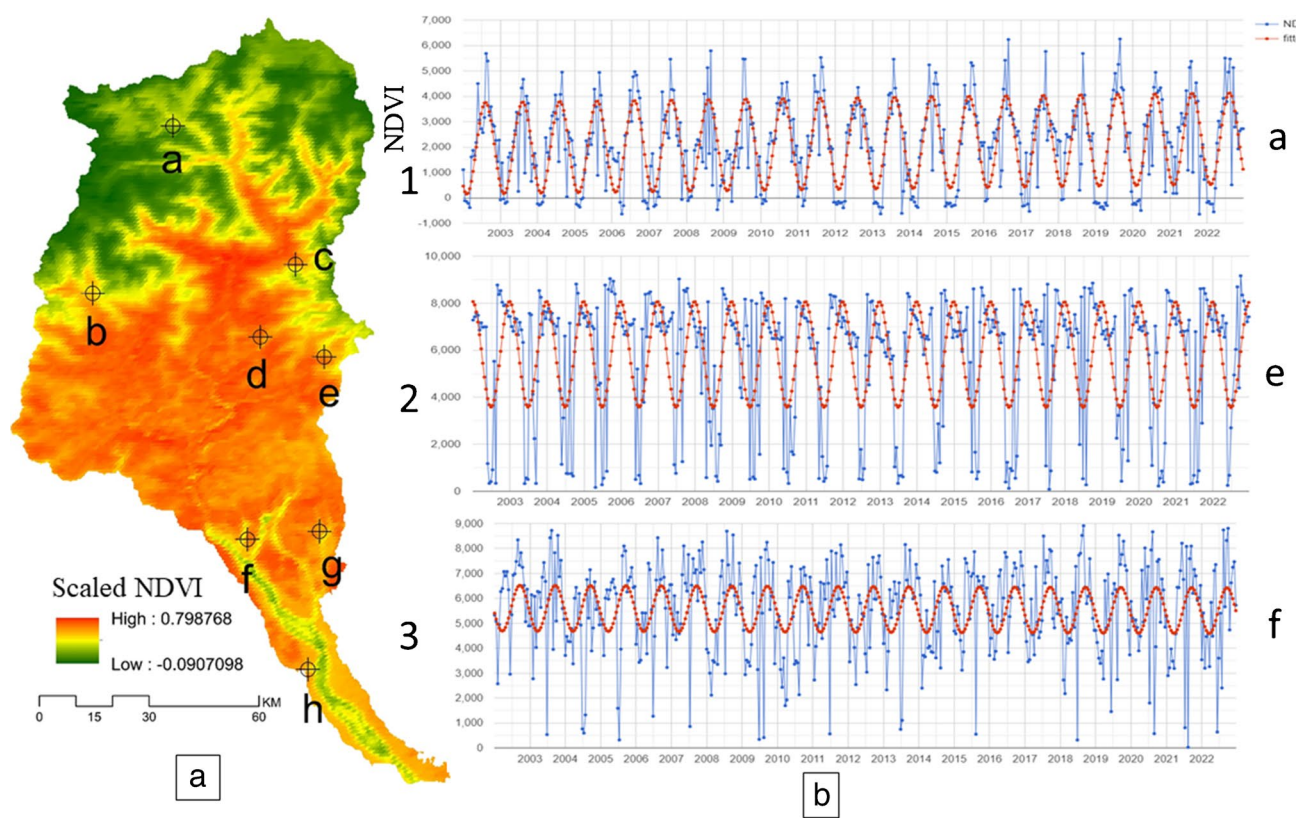


Fig. 8 Checking and validating site-specific VCC: **a** VCC at negative z -score trend (a) Khangchendzonga National Park (NP) (Sikkim), (b) Yuksom (Sikkim), (c) lower Chungthang valley (Sikkim), (d) Gangtok (Sikkim), (e) Kupup Valley (Sikkim), (f) Odlabari (West Bengal), (g) Malbazar (West Bengal), and (h) Jalpaiguri (West Bengal); **b** harmonic seasonality trend of NDVI (1) Khangchendzonga National Park, (2) Kupup Valley, and (3) Odlabari

gal), (g) Malbazar (West Bengal), and (h) Jalpaiguri (West Bengal)

Table 3 Summary of OSL and GWR model results

Metric	Stepwise model	Interaction model	Full OLS model	GWR model
Adjusted R^2	0.9117	0.874	0.916	0.941
Residual squares	-	-	3.811	200,825,219.778
Residual std. dev. (sigma)	-	-	0.080	578.540
AICc	-	-	-1265.179	7633.153
Significant predictor count	24	Limited (interactions)	28	-
Multicollinearity issues	Reduced	Some interactions	Present and resolved	Managed via spatial weights

Source: computed by the authors

indicating the relationships between the clustering pattern and the nine environmental factors.

Comparison of OSL and GWR model in terms of spatial auto-correlation.

The OLS model results reveal that 17.75% of pixels showed no discernible clustering (Fig. 10a), while 69% exhibited significant high–high clusters, indicating a spatial concentration of high predicted NDVI values. Conversely, 30.75% displayed significant low–low clusters, with 1.25% showing mixed clusters of adjacent high and low NDVI

values. These patterns highlight distinct spatial distributions of vegetation health, aiding in identifying areas with similar characteristics or underlying influencing factors. The GWR model predicted that 7.5% of pixels were not significant, while 60.75% formed high–high clusters and 48.25% showed low–low clusters (Fig. 10b), demonstrating a concentration of similar NDVI values. Additionally, local R^2 clustering in the GWR model (Fig. 10c) provided further insights into spatial relationships. The OLS model identified significant relationships in 77% of pixels ($p < 0.001$,

Fig. 9 Regression model and hotspot analysis outcomes: **a** distribution of standard residuals of OSL (linear) regression model, **b** distribution of standard residuals of GWR model, **c** IDW stretch of standard error of GWR model, and **d** clustering features (Getis-Ord G_i^*) of temporal trends in vegetation cover

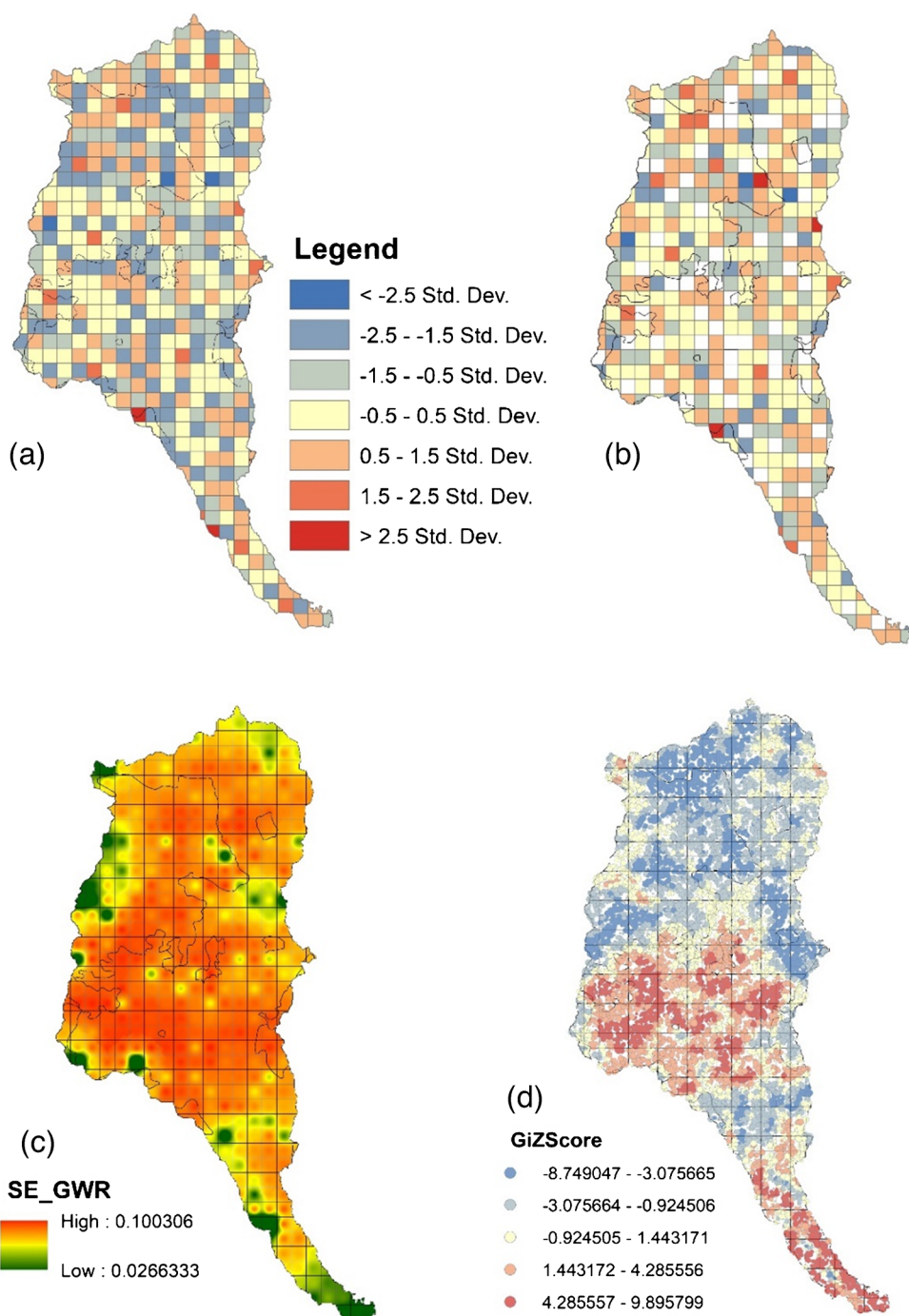


Fig. 10d), while the GWR model captured 97% ($p < 0.001$, Fig. 9e). The Univariate Moran's I analysis with LISA clustering summarizes (a) NDVI clustering in OLS, (b) NDVI clustering in GWR, (c) local R^2 clustering in GWR, (d) p -value clustering in OLS, and (e) p -value clustering in GWR, underscoring the predictive strength of both models. The GWR model revealed fewer but significant clusters, while the OLS model captured more high–high and low–low clusters, with strong statistical significance ($p < 0.001$) in both models.

Seasonal and specific trends of change

The fitted model data follows a cyclic pattern resembling a sine curve, suggesting that there is a recurring seasonal trend in the NDVI values over the years. The cyclic pattern approaches near '0', suggesting that the vegetation index experiences a significant decline during specific time periods, reaching values close to zero. This could be an indication of vegetation stress, reduced vegetation cover, or unfavourable environmental conditions affecting plant

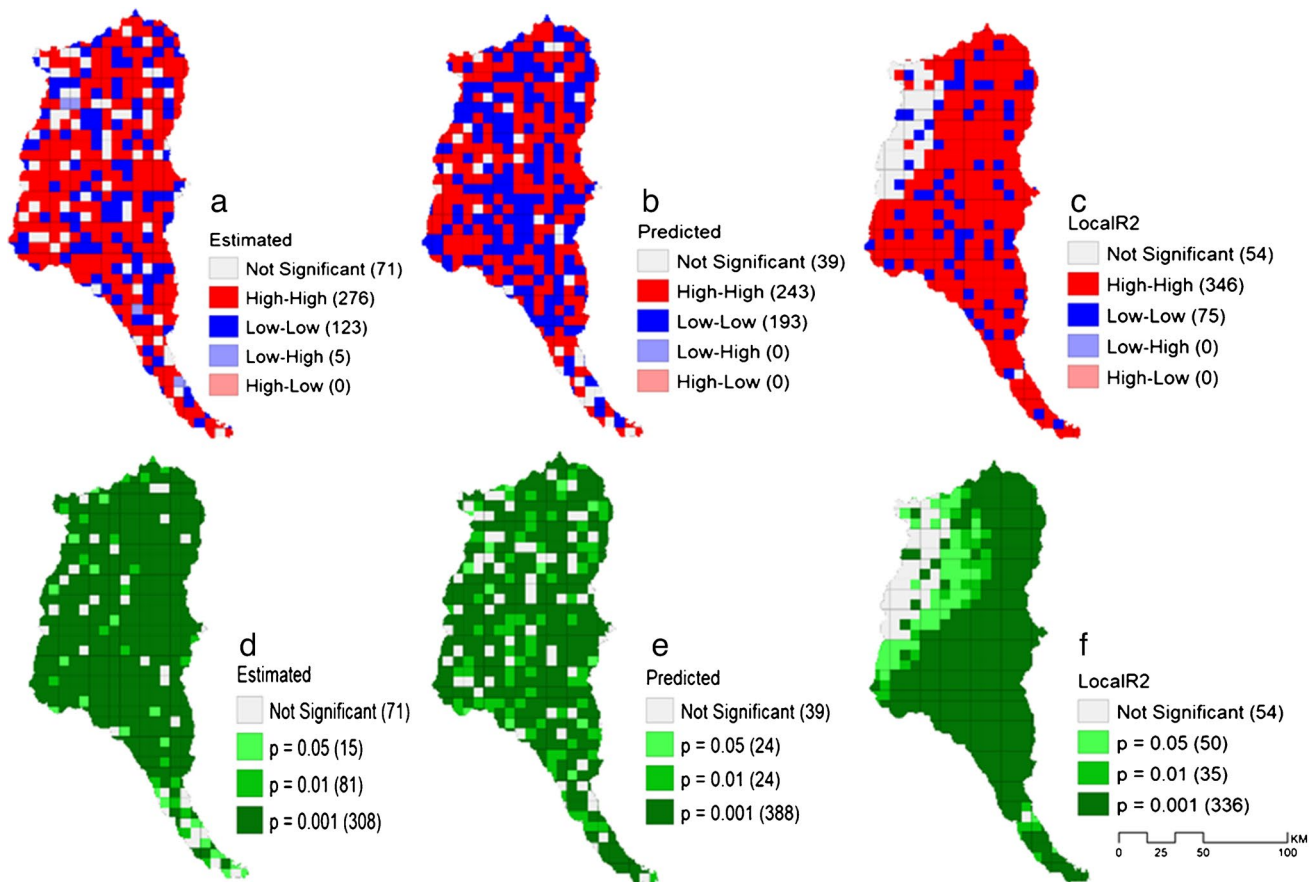


Fig. 10 Outcomes of univariate Moran's I analysis with LISA clustering: **a** clustering of estimated NDVI in OSL model, **b** clustering of estimated NDVI in GWR model, **c** clustering of local R^2 in GWR

model, **d** clustering of p -values in OSL model, **e** clustering of p -values in GWR model, and **f** clustering of p -values of local R^2 in GWR model

growth. The observed NDVI values range from 0 to 9000, indicating high fluctuations in dynamic vegetation seasonality. The validation points in the middle part of the basin exhibit high seasonal variation of NDVI from 2002 to 2022, but the points in the lower part of the basin do not show significant seasonality. The Mann–Kendall time series analysis of NDVI z -values across the entire basin also indicates a negative trend, confirming the declining vegetation activity. Sample points were mostly selected within the basin where the Sen's Slope (a measure of trend) is negative. This indicates a decreasing trend in NDVI values over time in these areas. The Mann–Kendall time series analysis of NDVI z -values across the entire basin also indicates a negative trend, confirming the declining vegetation activity. In the upper Teesta basin, grassland segments show a negative z -value trend. Below Chungthang, both woody savannah and grassland segments exhibit a negative z -value trend. Surrounding Nathang valley, there is a slightly negative z -value trend observed in woody savannah (Fig. 15b). In the east, near Kupup valley, there is a negative z -value trend in Evergreen Broadleaf Forests (Fig. 15f). At the piedmont section,

negative z trends are observed in both Evergreen Broadleaf Forests and Savannah land cover categories. Near Jalpaiguri town, Urban and Built-up Lands (Fig. 16), along with crop-lands and grasslands, show the same negative z -value trend (Fig. 8a and b). Overall, the findings suggest a declining trend in vegetation activity and NDVI values in the lower part of the Teesta basin. This trend is supported by negative Sen's Slopes, negative z -values, and the lack of pronounced seasonality in NDVI changes. The specific land cover categories also exhibit negative trends in their respective areas.

Role of human-driven factors

Based on the results generated by the Boosted Regression Tree (BTR) model, we can comment on the following role of Partial Dependency Plots (PDP) (Fig. 11a, b, c, d, and e), i.e., (a) Distance to Urban: The PDP shows a sharp rising tendency in the predicted response (z -value) between 4000 and 5000 m distance to urban centres. This suggests that as the distance to urban areas increases within this range, the model predicts a significant increase in the

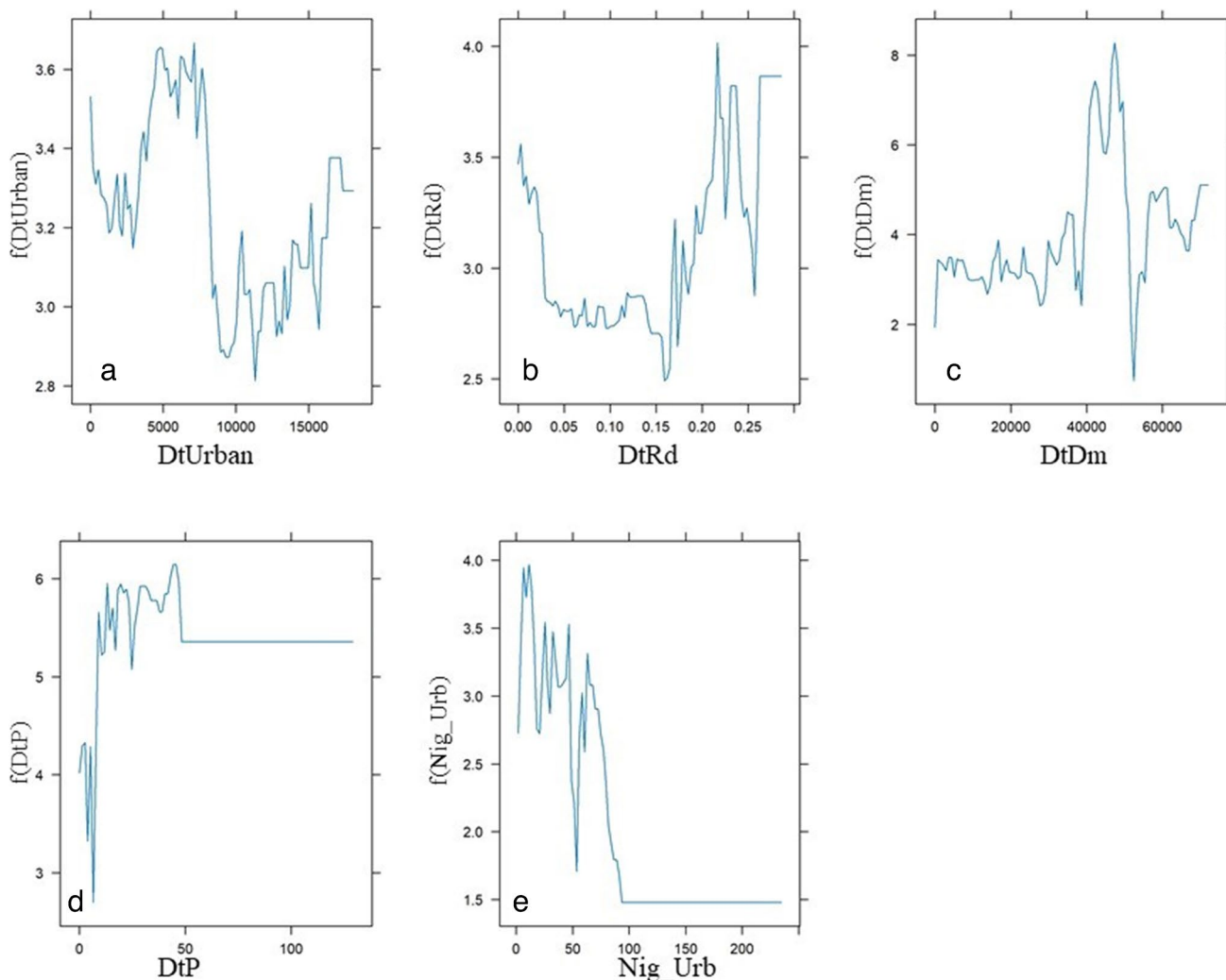


Fig. 11 Partial dependency plots (PDP) of human driven explanatory variables in the BRT model: **a** distance to urban centres, **b** distance to road, **c** distance to dam, **d** distance to population, and **e** distance to urban centres from night imagery

response variable (NDVI z -value). (b) Road Proximity: The PDP indicates that the model poorly predicts the response variable (NDVI z -value) in the range of 0.10 to 0.15 raster distance (Euclidean) for road proximity. However, as the distance increases beyond this range, the model's predictions gradually improve. (c) Distance to Dam: The PDP shows a bi-modal distribution, indicating that the model predicts the response variable well at certain ranges of distance to dams. (d) Population Proximity Raster: Overall, the predictor variable for population proximity plays a significant role in predicting the change in the response variable (NDVI z -value) based on the PDP. (e) Night Time Urban Patches: The PDP suggests that as the distance from urban patches increases, the model's predictor becomes less certain in predicting the change in the response variable (NDVI z -value).

According to the relative influence values, ‘Population Proximity’ has the highest relative influence (44.11%),

followed by ‘Distance to Dam’ (19.48%), ‘Night Time Urban Patches proximity’ (18.76%), ‘Road Proximity’ (9.28%), and ‘Urban proximity’ (8.37%). The BRT model displays a correlation between the training data and the predicted response of 0.784, which indicates a moderately strong correlation between the predicted response and the training data's actual response variable. The correlation between the predicted response and the actual response variable in the cross-validation data is 0.682, which points to a slightly weaker correlation (Table 4). Interaction patterns examine the direction of the interaction effect between the human-driven variables (Fig. 12a, b, c, d, e, and f). The first interaction suggests that the effect of roads on the outcome variable (NDVI) is stronger in areas that are closer to urban centres. The second and third interactions highlight the influence of specific geographical or contextual factors (unknown) on the relationship between variables. The other interactions

indicate that the observed interaction effect is unlikely to occur by chance. Lastly, the interaction between distance to population and road both creates a significant influence on the outcome variable (Fig. 12).

The results indicate that certain predictor variables, such as population proximity, distance to dams, and night-time urban patches, have a significant influence on predicting the response variable (NDVI z -value). The model performs well

Table 4 Arguments of running BRT model with relative influence of the predictors

Argument	Input	Variables in BRT	Relative influence (%)
X	Human-driven variables	DtP	44.11
Y	Response variable-NDVI	DtDm	19.48
Number of tree	1000	Nig_Urb	18.76
Family	Gaussian	DtRd	9.28
Tree Complexity	5	DtUrban	8.37
Shrinkage	0.03	Training data correlation	0.784
Bag fraction	0.5	Cross-validation correlation	0.682
Maximum number of trees	4		

Source: computed by the authors

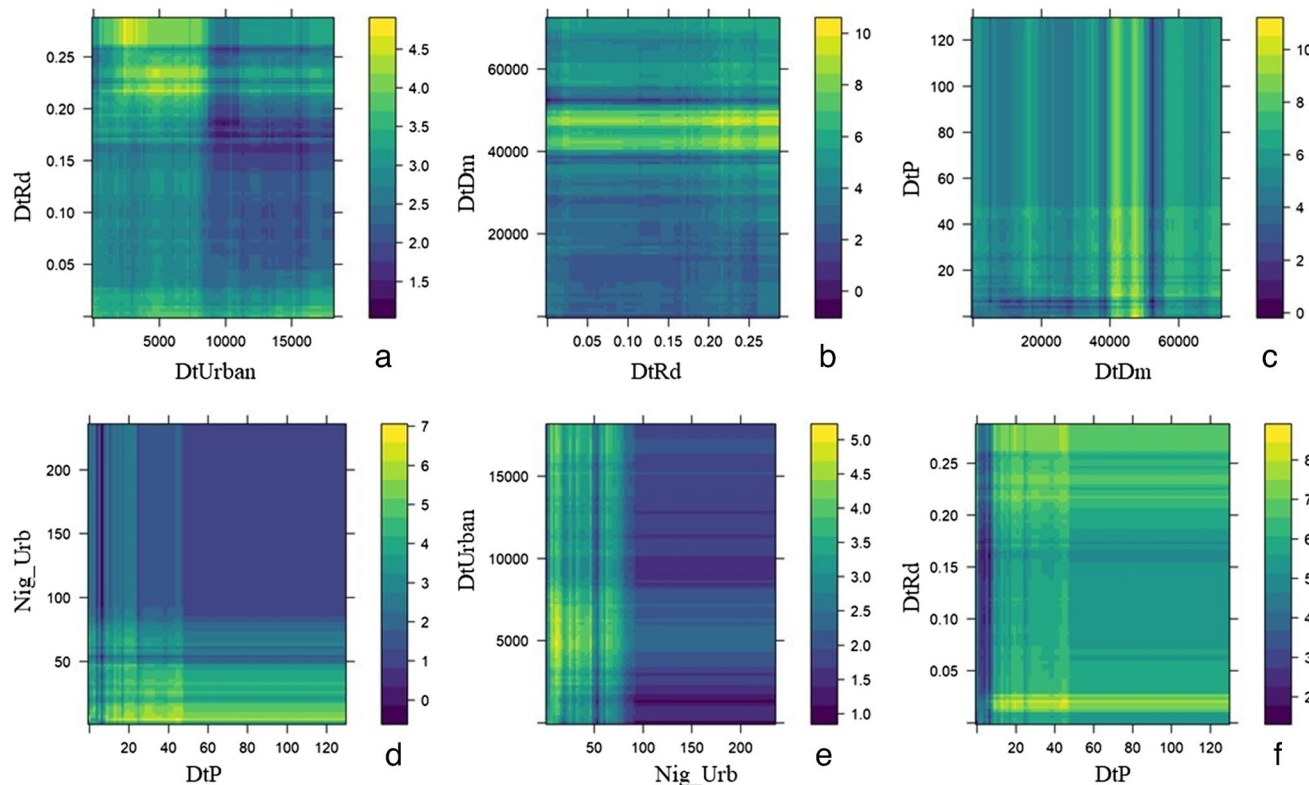


Fig. 12 Interaction plots of human-driven factors: (a) less distance from urban centres causes greater interaction with roads, (b) interaction in more location specific, (c) within a specific distance from the dams and increasing distance from population VCC is more pronounced, (d) weak interaction, (e) contradictory interaction between distance to night time and Landsat imagery driven urban centres on VCC, (f) high significant interaction between the driver variables.

nounced, (d) weak interaction, (e) contradictory interaction between distance to night time and Landsat imagery driven urban centres on VCC, (f) high significant interaction between the driver variables.

in some ranges of predictor variables, but there is room for improvement as applied over a wide basin area.

Discussion

A previous study on persistent negative changes in seasonal greenness over different forest types in India utilized the Mann–Kendall test and Sen's slope estimator instead of the Ordinary Least Square (OLS) method for analysing forest greenness trends due to their robustness in handling noisy, outlier-laden, or incomplete time series data. The Mann–Kendall test effectively identifies trends in the data, regardless of linearity, making it suitable for detecting both gradual and persistent changes in vegetation

greenness from 2001 to 2014. Sen's slope estimator complements this by robustly estimating the magnitude of these trends, providing a reliable median value even in the presence of data anomalies. These methods ensure accurate trend analysis in ecological studies where data irregularities are common (Chakraborty et al. 2018). The analysis of non-parametric trend (Mann–Kendall) and Sen's slope estimators for a 20-year period reveals interesting patterns in the vegetation dynamics within the study area. In Kangchendzonga National Park, there is a gradual transition from a negative to a positive trend in terms of Sen's slope, indicating a shift towards positive vegetation growth (Fig. 13a). This trend is consistent towards the eastern part of the park (Fig. 13b). Similar observations can be made in Singalila National Park, where the Sen's slope

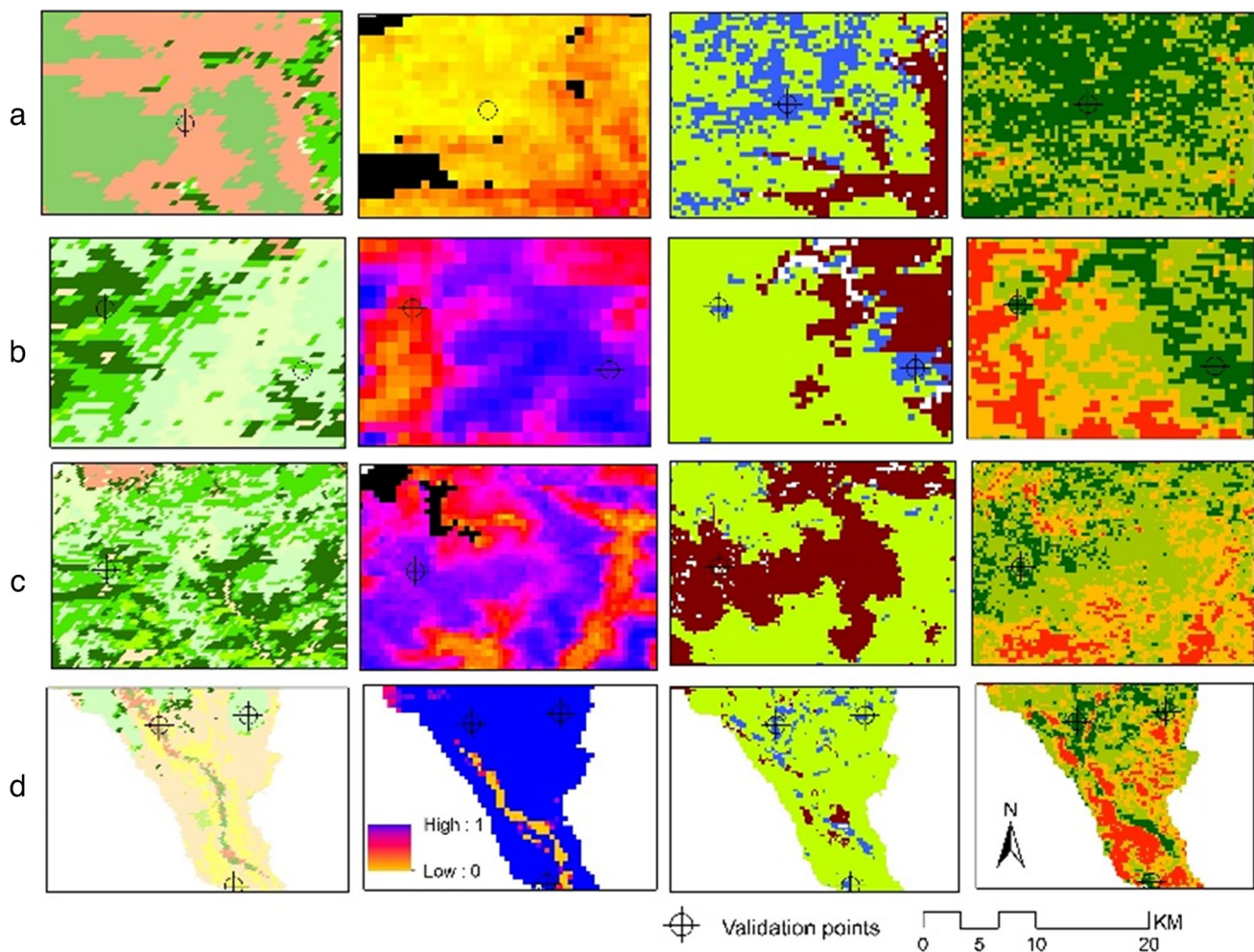


Fig. 13 Point specific comparison of various raster layers on negative z -score classes (from left to right: Landover, sensitivity of seasonal change of VC, Sen's slope and z -value of the Mann–Kendall trend) considering VCC: **a** the positive Sen's slope of dependency on x variables with less seasonal dynamics of broad needle leaf forests (Khangchendzonga National Park), **b** transitional VCC between short distance from mixed to deciduous needle leaf forest, changing sea-

sonality and positive to negative Sen's slope conversion (Gangtok to Kupup valley), **c** Moderate seasonal VCC with positive trend of Sen's slope in the transition zone of Evergreen broadleaf forest to shrubland (Yuksom), and **d** changing woody savannah to grassland with high seasonal trend of VCC and negative Sen's slope trend (Odlabari, piedmont zone)

also shows a transition from negative to positive, suggesting an improvement in vegetation conditions. A notable change in Vegetation Cover Change (VCC) is observed in Kyongnosla Alpine Wildlife Sanctuary, indicating a sudden shift in vegetation dynamics. On the other hand, Neora Valley National Park exhibits a consistent increase in VCC over the 20-year period, indicating vegetation growth and potentially favourable environmental conditions. The

significant p -values obtained from the Mann–Kendall trend analysis suggest a pronounced monotonic change in most of the Wildlife Sanctuaries (WLS) and National Parks (Fig. 14b and e). This indicates progress towards vegetation gain in these areas, except for the high-altitude regions of Kangchendzonga and Singalila National Parks, which are predominantly covered with snow throughout the year. Overall, the non-parametric trend analysis

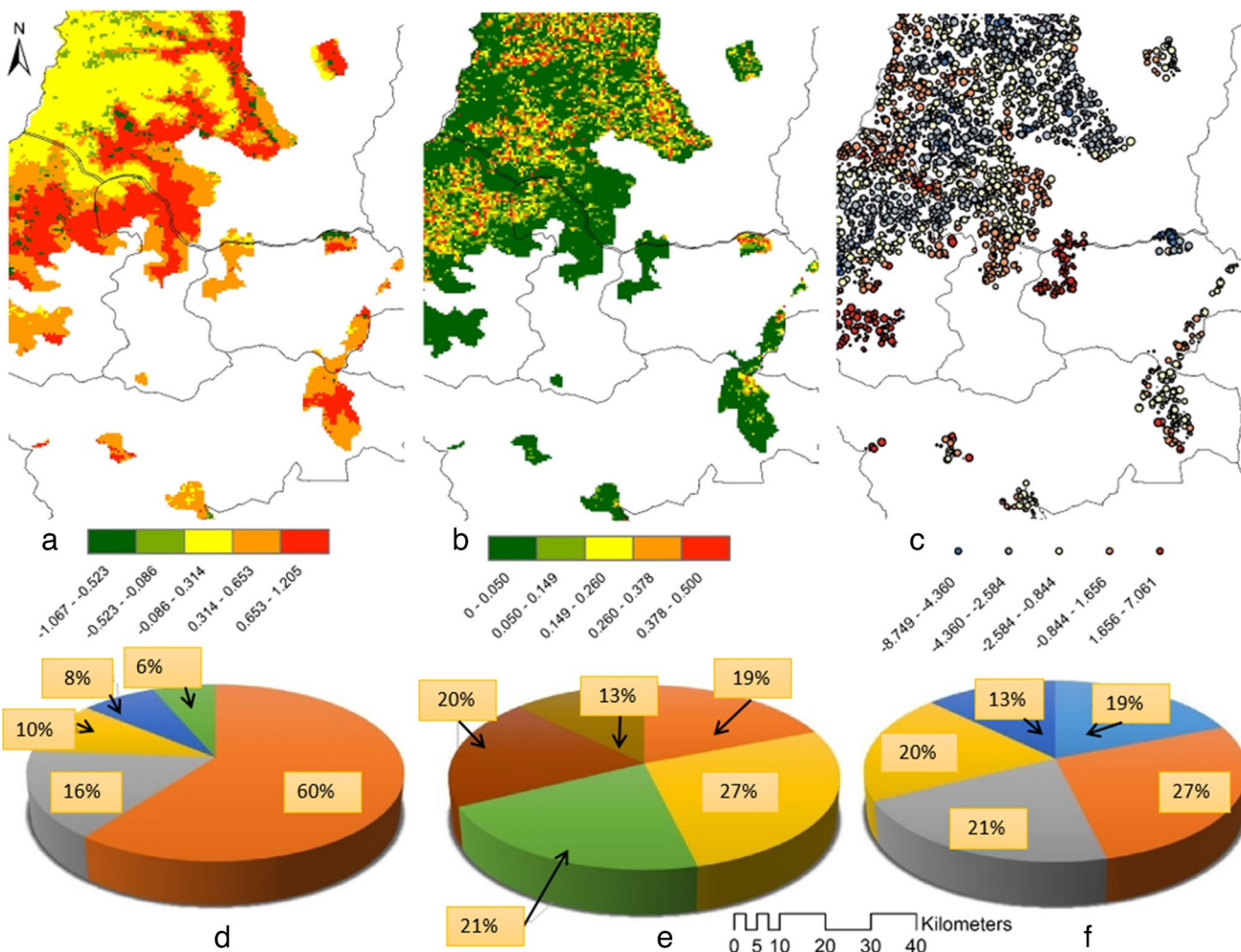


Fig. 14 Path analysis with different trend and cluster outcomes within National Parks (NP) and Wild-life sanctuaries (WLS): **a** Sen's slope, **b** p -value, **c** GI z -score, **d** areal distribution of Sen's slope, **e** areal distribution of p -value, and **f** areal distribution of GI z -scores

Table 5 Area coverage of various important trend parameters to justify VCC (data within protected forest areas)

Gi z -score classes	Area (%)	p -value (MK trend raster) classes	Area (%)	Sen's slope classes	Area (%)
-8.75 to -3.07	18.99	0 to 0.043	60.27	-1.067 to -0.523	2.6
-3.07 to -0.92	27.23	0.043 to 0.135	15.91	-0.523 to -0.086	5.2
-0.92 to 1.44	21.36	0.135 to 0.245	9.86	-0.086 to -0.314	31.18
1.44 to 4.28	19.65	0.245 to 0.368	7.57	0.314 to 0.653	33.90
4.28 to 9.89	12.79	0.368 to 0.500	6.37	0.653 to 1.205	26.94

Source: computed by the authors



Fig. 15 Field photographs portraying the reality and model validation: **a** peri-glacial grasslands of Khangchendzonga National Park (North Sikkim); **b** Yumthang valley near Shingba (Rhododendron) WLS (North Sikkim); **c** development of home-stay tourism in

Nathang Valley (East Sikkim); **d** trek through Barsey Rhododendron wild life sanctuary (West Sikkim); **e** patches of mixed forest at Kupup valley; and **f** famous Rhododendron (*Rhododendron niveum*) trek through Singalila National Park (Darjeeling, West Bengal)

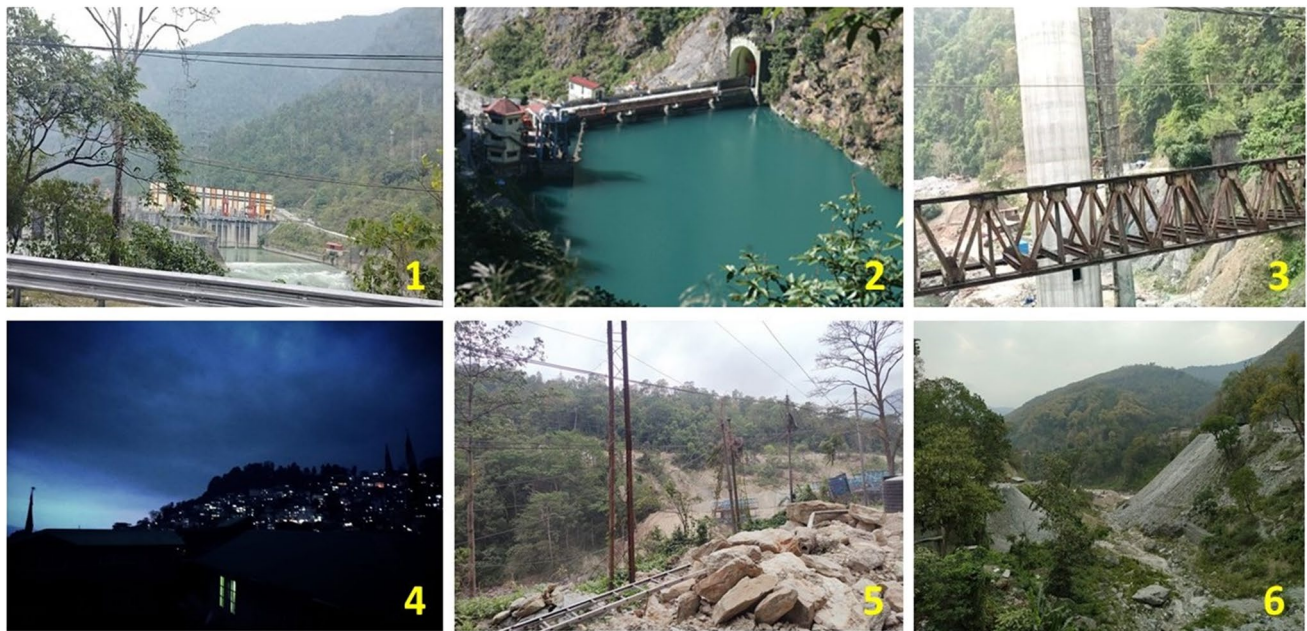


Fig. 16 Field photographs with signs of anthropogenic influences within the basin: **a** Teesta Low Dam IV near Kalijhora (West Bengal); **b** Rangit dam across a major tributary of Teesta (South Sikkim); **c** pillar construction on river bed part of new Sevok-Rongpo railway;

d night time side view of Gangtok town (East Sikkim); **e** new project of widening National Highway 10 for strategic reasons; and **f** hill top flattening for new road construction near Rangpo (South Sikkim)

of NDVI using the Mann–Kendall trend and Sen's slope estimators (Table 5) provides valuable insights into the long-term vegetation dynamics and highlights areas of

vegetation improvement and potential ecological significance. In Yuksom, there is moderate seasonal VCC with a positive trend of Sen's slope in the transition zone of

evergreen broadleaf forest to shrubland (Fig. 13c). Conversely, in Odlabari, located in the piedmont zone, there is a changing trend from woody savannah to grassland with a high seasonal trend of VCC and a negative Sen's slope trend (Fig. 13d). The variability in VCC across these regions underscores the critical need to consider localized ecological and climatic factors when evaluating environmental changes. These insights are crucial for formulating region-specific conservation strategies and understanding the broader implications of climate change and human activities on diverse ecosystems. A previous study identified significant declines in forest greenness using MODIS NDVI data from 2001 to 2014, across various Indian forest types, particularly in core areas of forests like tropical moist and dry deciduous regions. Key reductions were also noted in protected areas like the Simlipal and Rajaji wildlife sanctuaries. Gi* statistics were utilized for hotspot analysis, highlighting areas with the most severe greenness declines, crucial for targeted conservation and climate change actions (Chakraborty et al. 2018). The Gi *z-score* analysis reveals a concentration of significant negative values, indicating a decreasing trend in vegetation health (NDVI) within the basin. Approximately 67.58% of the area shows negative trends (Table 5), suggesting a decline in vegetation over the 20-year period. Khangchendzonga National Park, Fambong Lho Wildlife Sanctuary, Barsey Rhododendron Wildlife Sanctuary, and Maenam Wildlife Sanctuary experience significant negative changes in NDVI. Portions of Neora Valley National Park and the piedmont zone of Darjeeling-Sikkim Himalaya also show negative trends. These findings highlight areas of concern for conservation and management efforts. The greenness index (GI) values in this range are higher than the average, for instance, at Fambong Lho Wildlife Sanctuary and Barsey Rhododendron Wildlife Sanctuary. However, in other protected areas, the pattern of the standard error distribution is more random.

A comparison of negative *z-score* classes was made for validation (total 8 points) using various raster layers, considering VCC. The results showed positive Sen's slope dependency on explanatory variables in broad needle leaf forests (BNLF) in high mountain tracts (Khangchendzonga National Park) (Fig. 14a), moderate seasonal VCC with positive slope in evergreen broadleaf forest (EBLF) transition zones to Yuksom (within Khangchendzonga National Park and Barsey Rhododendron Wildlife Sanctuary) (Fig. 14b), for protected forest regions, the area percentage of GI *z-score* value ranges from 1.44 to 4.28, with a 19.65% total area (Fig. 14c), transitional VCC between mixed and deciduous needle leaf forests from Gangtok to far east (Fig. 14d), and finally, high seasonal VCC and negative slope trends can be observed within a transition zone from Woody Savannah (WS) to Grassland (G) over the piedmont section (Fig. 14e).

Conclusion

The extensive model analysis of the Teesta Basin in this study has illuminated the intricate dynamics of vegetation cover change (VCC), emphasizing the significant role of both environmental and human-driven factors (Figs. 15 and 16). The findings from the OSL Regression model indicate that land use, proximity to urban areas, roads, dams, elevation, and slope are crucial determinants of VCC, while factors like land surface temperature and night-time urban centres have a lesser impact. The Geographically Weighted Regression (GWR) analysis has further highlighted the spatial variations in these relationships, underscoring the importance of localized approaches in understanding VCC. Particularly striking is the discovery of recurring seasonal trends in vegetation activity, as evidenced by cyclic patterns in NDVI values, albeit with periods of decline indicating stress or unfavourable conditions. This cyclical nature of vegetation health, coupled with the significant influence of human activities like urban expansion and agriculture, especially in the lower regions of the basin, calls for a re-evaluation of current land management and conservation strategies. To address these challenges effectively, it is imperative to enhance conservation efforts, focusing particularly on areas showing negative trends. This includes adopting sustainable urban planning that harmonizes development with ecological preservation. The role of local communities cannot be overstated in this regard—their involvement is crucial for the successful implementation of sustainable practices. Moreover, the study suggests the necessity for ongoing monitoring and further research to gain a more nuanced understanding of the various factors impacting VCC. This will aid in the formulation of more targeted and effective conservation strategies, tailored to the unique characteristics of different regions within the Teesta Basin. In conclusion, this study serves as a clarion call for a balanced approach that combines conservation, sustainable development and community participation to safeguard and enhance the vegetation cover in the Teesta Basin, thus ensuring the health and resilience of its ecosystems.

Author contribution Debarshi Ghosh: Conceptualization, data curation, formal analysis, writing and original draft preparation, and visualization. Apurba Sarkar: methodology, software, validation, writing-review and editing, and supervision. Sanjoy Mandal: software and validation.

Data availability Not applicable.

Declarations

Ethics approval and consent to participate All authors have read, understood, and complied as applicable with the statement on the “Ethical Responsibilities of Authors” as found in the Instructions for Authors.

Conflict of interest The authors declare no competing interests.

References

- Abd El-Kawy OR, Rød JK, Ismail HA, Suliman AS (2011) Land use and land cover change detection in the western Nile Delta of Egypt using remote sensing data. *Appl Geogr* [internet] 31(2):483–494. <https://doi.org/10.1016/j.apgeog.2010.10.012>
- Abdollahi S, Pourghasemi HR, Ghanbarian GA, Safaeian R (2019) Prioritization of effective factors in the occurrence of land subsidence and its susceptibility mapping using an SVM model and their different kernel functions. *Bull Eng Geol Environ* 78(6):4017–4034. <https://doi.org/10.1007/s10064-018-1403-6>
- Baeza S, Paruelo JM (2020) Land use/land cover change (2000–2014) in the rio de la plata grasslands: an analysis based on MODIS NDVI time series. *Remote Sens* 12(3):1–22. <https://doi.org/10.3390/rs12030381>
- Bento VA, Gouveia CM, Dacamara CC, Libonati R, Trigo IF (2020) The roles of NDVI and land surface temperature when using the vegetation health index over dry regions. *Glob Planet Change* [Internet]. 190(July 2019):103198. <https://doi.org/10.1016/j.gloplacha.2020.103198>
- Bokusheva R, Kogan F, Vitkovskaya I, Conradt S, Batyrbayeva M (2016) Satellite-based vegetation health indices as a criteria for insuring against drought-related yield losses. *Agric for Meteorol* [internet] 220:200–206. <https://doi.org/10.1016/j.agrformet.2015.12.066>
- Chakraborty T, Ghosh P (2010) The geomorphology and sedimentology of the Tista megafan, Darjeeling Himalaya: implications for megafan building processes. *Geomorphology* 115(3–4):252–266. <https://doi.org/10.1016/j.geomorph.2009.06.035>
- Chakraborty A, Seshasai MVR, Reddy CS, Dadhwal VK (2018) Persistent negative changes in seasonal greenness over different forest types of India using MODIS time series NDVI data (2001–2014). *Ecol Indic* 85(March 2017):887–903. <https://doi.org/10.1016/j.ecolind.2017.11.032>
- Chamberlain DA, Phinn SR, Possingham HP (2021) Mangrove forest cover and phenology with landsat dense time series in central Queensland, Australia. *Remote Sens* 13(15):1–26. <https://doi.org/10.3390/rs13153032>
- Chen Z, Hu C, Muller-Karger F (2007) Monitoring turbidity in Tampa Bay using MODIS/Aqua 250-m imagery. *Remote Sens Environ* 109(2):207–220. <https://doi.org/10.1016/j.rse.2006.12.019>
- Chen S, Han L, Chen X, Li D, Sun L, Li Y (2015) Estimating wide range total suspended solids concentrations from MODIS 250-m imageries: an improved method. *ISPRS J Photogramm Remote Sens* 99:58–69. <https://doi.org/10.1016/j.isprsjprs.2014.10.006>
- Choudhury G (2016) Impact of hydropower on mountain communities in Teesta Basin of Eastern Himalaya, India. [place unknown]: Elsevier. <https://doi.org/10.1016/B978-0-444-63787-1.00006-8>
- Chughtai AH, Abbasi H, Karas IR (2021) A review on change detection method and accuracy assessment for land use land cover. *Remote Sens Appl Soc Environ* 22(February):100482. <https://doi.org/10.1016/j.rsase.2021.100482>
- Cui C, Zhang W, Hong ZM, Meng LK (2020) Forecasting NDVI in multiple complex areas using neural network techniques combined feature engineering. *Int J Digit Earth* 13(12):1733–1749. <https://doi.org/10.1080/17538947.2020.1808718>
- De Beurs KM, Henebry GM (2005) A statistical framework for the analysis of long image time series. *Int J Remote Sens* 26(8):1551–1573. <https://doi.org/10.1080/01431160512331326657>
- de Jong R, de Bruin S, de Wit A, Schaepman ME, Dent DL (2011) Analysis of monotonic greening and browning trends from global NDVI time-series. *Remote Sens Environ* 115(2):692–702. <https://doi.org/10.1016/j.rse.2010.10.011>
- Defries R, Hansen M, Townshend J (1995) Global Discrimination of land cover types from metrics derived from AVHRR Pathfinder data. *Remote Sens Environ* 222(March):209–222
- Deng X, Li Z, Huang J, Shi Q, Li Y (2013) A revisit to the impacts of land use changes on the human wellbeing via altering the ecosystem provisioning services. *Adv Meteorol* 2013. <https://doi.org/10.1155/2013/907367>
- Detsch F, Otte I, Appelhans T, Hemp A, Nauss T (2016) Seasonal and long-term vegetation dynamics from 1-km GIMMS-based NDVI time series at Mt. Kilimanjaro, Tanzania. *Remote Sens Environ* 178:70–83. <https://doi.org/10.1016/j.rse.2016.03.007>
- Devi NB, Lepcha NT, Mahalik SS, Dutta D, Tsanglao BL (2021) Urban sacred grove forests are potential carbon stores: a case study from Sikkim Himalaya. *Environ Challenges* 4(March):100072. <https://doi.org/10.1016/j.envc.2021.100072>
- Devkota M, Hatfield G, Chintala R (2014) Effect of sample size on the performance of ordinary least squares and geographically weighted regression. *Br J Math Comput Sci* 4(1):1–21. <https://doi.org/10.9734/bjmcs/2014/6050>
- Eckert S, Hüslér F, Liniger H, Hodel E (2015) Trend analysis of MODIS NDVI time series for detecting land degradation and regeneration in Mongolia. *J Arid Environ* [internet] 113:16–28. <https://doi.org/10.1016/j.jaridenv.2014.09.001>
- Erdoğan S (2010) Modelling the spatial distribution of DEM error with geographically weighted regression: an experimental study. *Comput Geosci* 36(1):34–43. <https://doi.org/10.1016/j.cageo.2009.06.005>
- Feng D, Fu M, Sun Y, Bao W, Zhang M, Zhang Y, Wu J (2021) How large-scale anthropogenic activities influence vegetation cover change in China? A review. *Forests* 12(3):1–13. <https://doi.org/10.3390/f12030320>
- Filella I, Peñuelas J, Llorens L, Estiarte M (2004) Reflectance assessment of seasonal and annual changes in biomass and CO₂ uptake of a Mediterranean shrubland submitted to experimental warming and drought. *Remote Sens Environ* 90(3):308–318. <https://doi.org/10.1016/j.rse.2004.01.010>
- Filippone F, Valentini E, Xuan AN, Guerra CA, Wolf F, Andrzejak M, Taramelli A (2018) Global MODIS fraction of green vegetation cover for monitoring abrupt and gradual vegetation changes. *Remote Sens* 10(4). <https://doi.org/10.3390/rs10040653>
- Forest Declaration Assessment Partners (2022) Overarching forest goals: theme 1 assessment. Forest declaration assessment: are we on track for 2030? Climate Focus (coordinator and editor). Retrieved from <https://forestdeclaration.org/resources/overarching-forest-goals-theme-1-assessment/>
- Gandhi GM, Parthiban S, Thummali N, Christy A (2015) Ndvi: Vegetation change detection using remote sensing and GIS - a case study of vellore district. *Procedia Comput Sci* 57:1199–1210. <https://doi.org/10.1016/j.procs.2015.07.415>
- Ghosh K (2021) A framework to assess the benefits and challenges of ecosystem services of a reservoir-based wetland in the Himalayan foothills. *Environ Dev* 40(July):100669. <https://doi.org/10.1016/j.envdev.2021.100669>
- Gillespie TW, Ostermann-Kelm S, Dong C, Willis KS, Okin GS, MacDonald GM (2018) Monitoring changes of NDVI in protected areas of southern California. *Ecol Indic* 88(January):485–494. <https://doi.org/10.1016/j.ecolind.2018.01.031>
- Gu Y, Brown JF, Verdin JP, Wardlow B (2007) A five-year analysis of MODIS NDVI and NDWI for grassland drought assessment over the central Great Plains of the United States. *Geophys Res Lett* 34(6):1–6. <https://doi.org/10.1029/2006GL029127>
- Han JC, Huang Y, Zhang H, Wu X (2019) Characterization of elevation and land cover dependent trends of NDVI variations in the Hexi region, northwest China. *J Environ Manage* 232(June):

- 2018):1037–1048. <https://doi.org/10.1016/j.jenvman.2018.11.069>
- Hansen MC, Loveland TR (2012) A review of large area monitoring of land cover change using Landsat data. *Remote Sens Environ [internet]* 122:66–74. <https://doi.org/10.1016/j.rse.2011.08.024>
- Hansen MC, Potapov PV, Moore R, Hancher M, Turubanova SA, Tyukavina A, Thau D, Stehman SV, Goetz SJ, Loveland TR et al (2013) High-resolution global maps of 21st-century forest cover change. *Science (80-)* 342(6160):850–853. <https://doi.org/10.1126/science.1244693>
- Haque MI, Basak R (2017) Land cover change detection using GIS and remote sensing techniques: a spatio-temporal study on Tangar Haor, Sunamganj, Bangladesh. *Egypt J Remote Sens Sp Sci* 20(2):251–263. <https://doi.org/10.1016/j.ejrs.2016.12.003>
- Harris NL, Gibbs DA, Baccini A, Birdsey RA, de Bruin S, Farina M, Fatoyinbo L, Hansen MC, Herold M, Houghton RA et al (2021) Global maps of twenty-first century forest carbon fluxes. *Nat Clim Chang [internet]* 11(3):234–240. <https://doi.org/10.1038/s41558-020-00976-6>
- Holben BN (1986) Characteristics of maximum-value composite images from temporal AVHRR data. *Int J Remote Sens* 7(11):1417–1434. <https://doi.org/10.1080/01431168608948945>
- Huang S, Ming B, Huang Q, Leng G, Hou B (2017) A case study on a combination NDVI forecasting model based on the entropy weight method. *Water Resour Manag* 31(11):3667–3681. <https://doi.org/10.1007/s11269-017-1692-8>
- Huang S, Tang L, Hupy JP, Wang Y, Shao G (2021) A commentary review on the use of normalized difference vegetation index (NDVI) in the era of popular remote sensing. *J for Res [internet]* 32(1):1–6. <https://doi.org/10.1007/s11676-020-01155-1>
- Hulley G, Veraverbeke S, Hook S (2014) Thermal-based techniques for land cover change detection using a new dynamic MODIS multispectral emissivity product (MOD21). *Remote Sens Environ [internet]* 140:755–765. <https://doi.org/10.1016/j.rse.2013.10.014>
- Hussien K, Kebede A, Mekuriaw A, Beza SA, Erena SH (2023) Spatiotemporal trends of NDVI and its response to climate variability in the Abbay River Basin. *Ethiopia Heliyon* 9(3):e14113. <https://doi.org/10.1016/j.heliyon.2023.e14113>
- Jakubauskas ME, Legates DR, Kastens JH (2001) 2001_Jakubauskas_Etal_Time-Series. 67(4):461–470
- Jiang M, Tian S, Zheng Z, Zhan Q, He Y (2017) Human activity influences on vegetation cover changes in Beijing, China, from 2000 to 2015. *Remote Sens* 9(3):1–19. <https://doi.org/10.3390/rs9030271>
- Justice CO, Giglio L, Korontzi S, Owens J, Morisette JT, Roy D, Descloitres J, Alleaume S, Petitcolin F, Kaufman Y (2002) The MODIS fire products. *Remote Sens Environ* 83(1–2):244–262. [https://doi.org/10.1016/S0034-4257\(02\)00076-7](https://doi.org/10.1016/S0034-4257(02)00076-7)
- Kanade R, John R (2018) Topographical influence on recent deforestation and degradation in the Sikkim Himalaya in India; implications for conservation of East Himalayan broadleaf forest. *Appl Geogr* 92(February):85–93. <https://doi.org/10.1016/j.apgeog.2018.02.004>
- Karim MR, Thiel A (2017) Role of community based local institution for climate change adaptation in the Teesta riverine area of Bangladesh. *Clim Risk Manag* 17:92–103. <https://doi.org/10.1016/j.crm.2017.06.002>
- Klein I, Gessner U, Kuenzer C (2012) Regional land cover mapping and change detection in Central Asia using MODIS time-series. *Appl Geogr [internet]* 35(1–2):219–234. <https://doi.org/10.1016/j.apgeog.2012.06.016>
- Krishna AP (1996) Cover: Satellite remote sensing applications for snow cover characterization in the morphogenetic regions of upper tista river basin, sikkim himalaya. *Int J Remote Sens* 17(4):651–656. <https://doi.org/10.1080/01431169608949035>
- Kulkarni AV, Rathore BP, Singh SK, Bahuguna IM (2011) Understanding changes in the Himalayan cryosphere using remote sensing techniques. *Int J Remote Sens* 32(3):601–615. <https://doi.org/10.1080/01431161.2010.517802>
- Kundu A, Matin A, Mukul M (2012) Depositional environment and provenance of Middle Siwalik sediments in Tista valley, Darjeeling District Eastern Himalaya, India. *J Earth Syst Sci* 121(1):73–89. <https://doi.org/10.1007/s12040-012-0154-1>
- Lasaponara R (2006) On the use of principal component analysis (PCA) for evaluating interannual vegetation anomalies from Spot/Vegetation NDVI temporal series. *Ecol Model* 194(4):429–434. <https://doi.org/10.1016/j.ecolmodel.2005.10.035>
- Lawer EA, Baatuuwie BN, Ochire-Boadu K, Asante WJ, Lawer EA, Baatuuwie BN, Ochire-Boadu K, Asante WJ (2013) Preliminary assessment of the effects of anthropogenic activities on vegetation cover and natural regeneration in a moist semi-deciduous forest of Ghana. *Int J Ecosyst* 3(5):148–156. <https://doi.org/10.5923/j.ije.20130305.07>
- Li Z, Li X, Wei D, Xu X, Wang H (2010) An assessment of correlation on MODIS-NDVI and EVI with natural vegetation coverage in Northern Hebei Province, China. *Procedia Environ Sci* 2:964–969. <https://doi.org/10.1016/j.proenv.2010.10.108>
- Li Z, Huffman T, McConkey B, Townley-Smith L (2013) Monitoring and modeling spatial and temporal patterns of grassland dynamics using time-series MODIS NDVI with climate and stocking data. *Remote Sens Environ* 138:232–244. <https://doi.org/10.1016/j.rse.2013.07.020>
- Li D, Lu D, Zhao Y, Zhou M, Chen G (2021) Spatial patterns of vegetation coverage change in giant panda habitat based on MODIS time-series observations and local indicators of spatial association. *Ecol Indic* 124. <https://doi.org/10.1016/j.ecolind.2021.107418>
- Lin L, Li Q, Yang J, Han N, Chen G, Jin C, Xu X, Liu Z, Liu J, Luo S et al (2020) The associations of residential greenness with fetal growth in utero and birth weight: a birth cohort study in Beijing, China. *Environ Int* 141(December 2019):105793. <https://doi.org/10.1016/j.envint.2020.105793>
- Liu R, Shang R, Liu Y, Lu X (2017) Global evaluation of gap-filling approaches for seasonal NDVI with considering vegetation growth trajectory, protection of key point, noise resistance and curve stability. *Remote Sens Environ* 189:164–179. <https://doi.org/10.1016/j.rse.2016.11.023>
- Liu H, Zheng L, Yin S (2018) Multi-perspective analysis of vegetation cover changes and driving factors of long time series based on climate and terrain data in Hanjiang River Basin, China. *Arab J Geosci* 11(17). <https://doi.org/10.1007/s12517-018-3756-3>
- Manna S, Biswas S, Kundu R, Rakshit S, Gupta P, Barman S (2018) A statistical approach to predict flight delay using gradient boosted decision tree. *ICCID 2017 - Int Conf Comput Intell Data Sci Proc.* 2018-Janual 1–5. <https://doi.org/10.1109/ICCID.2017.8272656>
- Miller RL, McKee BA (2004) Using MODIS Terra 250 m imagery to map concentrations of total suspended matter in coastal waters. *Remote Sens Environ* 93(1–2):259–266. <https://doi.org/10.1016/j.rse.2004.07.012>
- Mishra PK, Rai A, Rai SC (2020) Land use and land cover change detection using geospatial techniques in the Sikkim Himalaya, India. *Egypt J Remote Sens Sp Sci* 23(2):133–143. <https://doi.org/10.1016/j.ejrs.2019.02.001>
- Mondal MSH, Murayama T, Nishikizawa S (2020) Assessing the flood risk of riverine households: a case study from the right bank of the Teesta River, Bangladesh. *Int J Disaster Risk Reduct* 51:101758. <https://doi.org/10.1016/j.ijdrr.2020.101758>
- Neeti N, Eastman JR (2011) A Contextual Mann-Kendall approach for the assessment of trend significance in image time series.

- Trans GIS 15(5):599–611. <https://doi.org/10.1111/j.1467-9671.2011.01280.x>
- Neeti N, Rogan J, Christman Z, Eastman JR, Millones M, Schneider L, Nickl E, Schmook B, Turner BL, Ghimire B (2012) Mapping seasonal trends in vegetation using AVHRR-NDVI time series in the Yucatán Peninsula, Mexico. *Remote Sens Lett* 3(5):433–442. <https://doi.org/10.1080/01431161.2011.616238>
- Nega W, Hailu BT, Fetene A (2019) An assessment of the vegetation cover change impact on rainfall and land surface temperature using remote sensing in a subtropical climate, Ethiopia. *Remote Sens Appl Soc Environ* [internet] 16 (September):100266. <https://doi.org/10.1016/j.rsase.2019.100266>
- Novillo CJ, Arrogante-Funes P, Romero-Calcerrada R (2019) Recent NDVI trends in mainland Spain: land-cover and phytoclimatic-type implications. *ISPRS Int J Geo-Information* 8(1):5–7. <https://doi.org/10.3390/ijgi8010043>
- Ohana-Levi N, Paz-Kagan T, Panov N, Peeters A, Tsoar A, Karnieli A (2019a) Time series analysis of vegetation-cover response to environmental factors and residential development in a dryland region. *Giscience Remote Sens* 56(3):362–387. <https://doi.org/10.1080/15481603.2018.1519093>
- Ohana-Levi N, Paz-Kagan T, Panov N, Peeters A, Tsoar A, Karnieli A (2019b) Time series analysis of vegetation-cover response to environmental factors and residential development in a dryland region. *Giscience Remote Sens* [internet] 56(3):362–387. <https://doi.org/10.1080/15481603.2018.1519093>
- Ojima DS, Galvin KA, Turner BL II (1994) The global impact of land-use change to understand global change, natural scientists must consider the social context influencing human impact on environment. *Bioscience* 44(5):300–304
- Padhee SK, Dutta S (2019) Spatio-temporal reconstruction of MODIS NDVI by regional land surface phenology and harmonic analysis of time-series. *Giscience Remote Sens* 56(8):1261–1288. <https://doi.org/10.1080/15481603.2019.1646977>
- Pal R, Pani P (2016) Recent changes in braided planform of the Tista River in the eastern lobe of the Tista Megafan, India. *Earth Sci India*. 9(2):104–113. <https://doi.org/10.31870/esi.09.2.2016.6>
- Pan F, Xie J, Lin J, Zhao T, Ji Y, Hu Q, Pan X, Wang C, Xi X (n.d.) Evaluation of climate change impacts on wetland vegetation in the Dunhuang Yangguan National Nature Reserve in Northwest China using Landsat derived NDVI. <https://doi.org/10.3390/rs10050735>
- Pei F, Zhou Y, Xia Y (2021) Application of normalized difference vegetation index (NDVI) for the detection of extreme precipitation change. *Forests* 12(5). <https://doi.org/10.3390/f12050594>
- Peng H, Wang S, Wang X (2008) Consistency and asymptotic distribution of the Theil-Sen estimator. *J Stat Plan Inference* 138(6):1836–1850. <https://doi.org/10.1016/j.jspi.2007.06.036>
- Piao S, Fang J, Zhou L, Guo Q, Henderson M, Ji W, Li Y, Tao S (2003) Interannual variations of monthly and seasonal normalized difference vegetation index (NDVI) in China from 1982 to 1999. *J Geophys Res Atmos* 108(14):1–13. <https://doi.org/10.1029/2002jd002848>
- Qin B, Zhu W, Wang J, Peng Y (2021) Understanding the relationship between neighbourhood green space and mental well-being: a case study of Beijing, China. *Cities*. 109(November 2020):103039. <https://doi.org/10.1016/j.cities.2020.103039>
- Ramanathan K, Thenmozhi M, George S, Anandan S, Veeraraghavan B, Naumova EN, Jeyaseelan L (2020) Assessing seasonality variation with harmonic regression: accommodations for sharp peaks. *Int J Environ Res Public Health*. 17(4). <https://doi.org/10.3390/ijerph17041318>
- Ranjan OJ, Rani U, Anand S, Pandey BW, Mukwada G, Escalante PD los R, Akyuz DE, Chaudhary A (2022) Spatial-temporal analysis of physio-climatic changes in Tawang- Chu River Basin, Eastern Himalaya in India. *Int J Ecol Environ Sci* 49(2). <https://doi.org/10.55863/ijees.2023.2626>
- Recuero L, Litago J, Pinzón JE, Huesca M, Moyano MC, Palacios-Orueta A (2019) Mapping periodic patterns of global vegetation based on spectral analysis of NDVI time series. *Remote Sens* 11(21):1–21. <https://doi.org/10.3390/rs11212497>
- Riihimäki H, Heiskanen J, Luoto M (2017) The effect of topography on arctic-alpine aboveground biomass and NDVI patterns. *Int J Appl Earth Obs Geoinf* 56:44–53. <https://doi.org/10.1016/j.jag.2016.11.005>
- Sarkar A, Roy L, Das S, Sengupta S (2021) Fluvial response to active tectonics: analysis of DEM-derived longitudinal profiles in the Rangit River Basin, Eastern Himalayas, India. *Environ Earth Sci* 80(7):1–22. <https://doi.org/10.1007/s12665-021-09561-2>
- Shimu SA, Aktar M, Afjal MI, Nitu AM, Uddin MP, Al Mamun M (2019) NDVI based change detection in Sundarban mangrove forest using remote sensing data. 2019 4th Int Conf Electr Inf Commun Technol EICT 2019 (December):1–5. <https://doi.org/10.1109/EICT48899.2019.9068819>
- Silveira EMDO, Espírito-Santo FDB, Acerbi-Júnior FW, Galvão LS, Withey KD, Blackburn GA, de Mello JM, Shimabukuro YE, Domingues T, Scolforo JRS (2019) Reducing the effects of vegetation phenology on change detection in tropical seasonal biomes. *GIScience Remote Sens*. 56(5):699–717. <https://doi.org/10.1080/15481603.2018.1550245>
- Simoniello T, Lanfredi M, Liberti M, Coppola R, Macchiato M (2008) Estimation of vegetation cover resilience from satellite time series. *Hydrol Earth Syst Sci* 12(3):1053–1064. <https://doi.org/10.5194/hess-12-1053-2008>
- Singh SP, Singh V, Skutsch M (2010) Rapid warming in the Himalayas: ecosystem responses and development options. *Clim Dev* 2(3):221–232. <https://doi.org/10.3763/cdev.2010.0048>
- Singh RP, Singh N, Singh S, Mukherjee S (2016) Normalized difference vegetation index (NDVI) based classification to assess the change in land use/land cover (LULC) in Lower Assam, India. *Int J Adv Remote Sens GIS* 5(1):1963–1970. <https://doi.org/10.23953/cloud.ijarsg.74>
- Sultana MR, Hassan Z, Paul SK (2018) Mitigation of erosion-induced disaster through indigenous practices: evidence from rural community of Teesta River bank. *J Life Earth Sci* 13(August 2019):22–31
- Sundriyal RC, Sharma E (1996) Anthropogenic pressure on tree structure and biomass in the temperate forest of Mamlay watershed in Sikkim. *For Ecol Manage* 81(1–3):113–134. [https://doi.org/10.1016/0378-1127\(95\)03657-1](https://doi.org/10.1016/0378-1127(95)03657-1)
- Taddei R (1997) Maximum value interpolated (MVI): a maximum value composite method improvement in vegetation index profiles analysis. *Int J Remote Sens* 18(11):2365–2370. <https://doi.org/10.1080/014311697217657>
- Talukdar S, Eibek KU, Akhter S, Ziaul S, Towfiqul Islam ARM, Mallick J (2021) Modeling fragmentation probability of land-use and land-cover using the bagging, random forest and random subspace in the Teesta River Basin, Bangladesh. *Ecol Indic* 126. <https://doi.org/10.1016/j.ecolind.2021.107612>
- Tambe S, Arrawatia ML, Sharma N (2011) Assessing the priorities for sustainable forest management in the Sikkim Himalaya, India: a remote sensing based approach. *J Indian Soc Remote Sens* 39(4):555–564. <https://doi.org/10.1007/s12524-011-0110-6>
- Tang Q, Wang J, Jing Z, Yan Y, Niu H (2021) Response of ecological vulnerability to land use change in a resource-based city, China. *Resour Policy* 74(September):102324. <https://doi.org/10.1016/j.resourpol.2021.102324>
- Traore SS, Forkuo EK, Traore PCS, Landmann T (2015) Assessing the inter-relationship between vegetation productivity, rainfall, population and land cover over the Bani River Basin in Mali (West Africa). *IOSR J Eng* 5(6):10–18

- Turubanova S, Potapov PV, Tyukavina A, Hansen MC (2018) Ongoing primary forest loss in Brazil, Democratic Republic of the Congo, and Indonesia. *Environ Res Lett* 13(7). <https://doi.org/10.1088/1748-9326/aacd1c>
- Vrielin A, de Beurs KM, Brown ME (2011) Variability of African farming systems from phenological analysis of NDVI time series. *Clim Change* 109(3–4):455–477. <https://doi.org/10.1007/s10584-011-0049-1>
- Wang SW, Gebru BM, Lamchin M, Kayastha RB, Lee WK (2020) Land use and land cover change detection and prediction in the kathmandu district of nepal using remote sensing and GIS. *Sustain* 12(9). <https://doi.org/10.3390/su12093925>
- Wellmann T, Schug F, Haase D, Pflugmacher D, van der Linden S (2020) Green growth? On the relation between population density, land use and vegetation cover fractions in a city using a 30-years Landsat time series. *Landsc Urban Plan* [internet] 202(May):103857. <https://doi.org/10.1016/j.landurbplan.2020.103857>
- Yan E, Wang G, Lin H, Xia C, Sun H (2015) Phenology-based classification of vegetation cover types in Northeast China using MODIS NDVI and EVI time series. *Int J Remote Sens* 36(2):489–512. <https://doi.org/10.1080/01431161.2014.999167>
- Yang L, Xian G, Klaver JM, Deal B (2003) Urban land-cover change detection through sub-pixel imperviousness mapping using remotely sensed data. *Photogramm Eng Remote Sens* 69(9):1003–1010. <https://doi.org/10.14358/PERS.69.9.1003>
- Yue S, Pilon P (2004) A comparison of the power of the t test, Mann-Kendall and bootstrap tests for trend detection. *Hydrol Sci J* 49(1):21–37. <https://doi.org/10.1623/hysj.49.1.21.53996>
- Zhan X, Sohlberg RA, Townshend JRG, DiMiceli C, Carroll ML, Eastman JC, Hansen MC, DeFries RS (2002) Detection of land cover changes using MODIS 250 m data. *Remote Sens Environ* 83(1–2):336–350. [https://doi.org/10.1016/S0034-4257\(02\)00081-0](https://doi.org/10.1016/S0034-4257(02)00081-0)
- Zhang Y, Ye A (2020) Spatial and temporal variations in vegetation coverage observed using AVHRR GIMMS and Terra MODIS data in the mainland of China. *Int J Remote Sens* [internet] 41(11):4238–4268. <https://doi.org/10.1080/01431161.2020.1714781>
- Zhang S, Lu XX, Higgitt DL, Chen CTA, Han J, Sun H (2008) Recent changes of water discharge and sediment load in the Zhujiang (Pearl River) Basin, China. *Glob Planet Change* 60(3–4):365–380. <https://doi.org/10.1016/j.gloplacha.2007.04.003>
- Zhang N, Zhang Y, Lu H (2011) Seasonal autoregressive integrated moving average and support vector machine models: prediction of short-term traffic flow on freeways. *Transp Res Rec* 2215:85–92. <https://doi.org/10.3141/2215-09>
- Zhao R, Liu X, Dong J, Zhao G, Manevski K, Andersen MN, Tang Q (2022) Human activities modulate greening patterns: a case study for southern Xinjiang in China based on long time series analysis. *Environ Res Lett* 17(4). <https://doi.org/10.1088/1748-9326/ac58a9>
- Zheng B, Myint SW, Thenkabail PS, Aggarwal RM (2015) A support vector machine to identify irrigated crop types using time-series Landsat NDVI data. *Int J Appl Earth Obs Geoinf* 34(1):103–112. <https://doi.org/10.1016/j.jag.2014.07.002>
- Zhou J, Jia L, Menenti M (2015) Reconstruction of global MODIS NDVI time series: performance of harmonic analysis of time series (HANTS). *Remote Sens Environ* 163:217–228. <https://doi.org/10.1016/j.rse.2015.03.018>

Springer Nature or its licensor (e.g. a society or other partner) holds exclusive rights to this article under a publishing agreement with the author(s) or other rightsholder(s); author self-archiving of the accepted manuscript version of this article is solely governed by the terms of such publishing agreement and applicable law.